Precambrian Research 411 (2024) 107526

Contents lists available at ScienceDirect

Precambrian Research

journal homepage: www.elsevier.com/locate/precamres

The basal Cambrian carbon isotope excursion revealed in the Central Iberian Zone, Spain

Kun Zhang [a,*], Graham A. Shields [a], Ying Zhou [a], Harald Strauss [b], Ulrich Struck [c], Sören Jensen [d]

[a] Department of Earth Sciences, University College London, WC1E 6BT, UK
[b] Institut für Geologie und Paläontologie, Westfälische Wilhelms-Universität Münster, 48149 Münster, Germany
[c] Museum für Naturkunde, Leibniz Institute for Evolution and Biodiversity Science, 10115 Berlin, Germany
[d] Área de Paleontología, Facultad de Ciencias, Universidad de Extremadura, 06006 Badajoz, Spain

ARTICLE INFO

Keywords:
Ediacaran
Cambrian
Carbon isotopes
Nitrogen isotopes

ABSTRACT

The causes of early metazoan diversification during the Ediacaran-Cambrian transition interval are controversial, partly because the global correlation of the Ediacaran-Cambrian boundary remains problematic due to a lack of unambiguous stratigraphic markers. Here we report geochemical data from two fossiliferous sections (Majada de Andaluz and Vía Verde) that straddle the Ediacaran-Cambrian interval in the Central Iberian Zone, Spain. Carbon isotope chemostratigraphy reveals a rise to a low positive $\delta^{13}C_{carb}$ plateau at the base of the Majada section, which is associated with the first appearance of *Cloudina* and a pristine Sr isotope value of 0.708512, suggesting that the lower Villarta Formation correlates with the terminal Ediacaran strata in China and Namibia. A prominent negative $\delta^{13}C_{carb}$ excursion is also revealed from the lower member of the Villarta Formation at Majada, likely corresponding to the global basal Cambrian carbon isotope excursion (BACE). Nitrogen isotope data from the correlative Vía Verde section reveal a similar trend to that found in coeval strata of South China, and indicate a change from predominantly anaerobic to aerobic nitrogen cycling in Central Iberia. By correlating sections in which both the BACE excursion and *Treptichnus pedum* are recognized, it appears that *T. pedum* is exclusively found above the BACE, which postdates the last appearance of *Cloudina* and a negative $\delta^{13}C_{carb}$ plateau. Further studies of sections with both fossil and isotopic control will help to constrain the timing and causation of Ediacaran-Cambrian bioradiations as well as their relationship to global carbon cycle perturbations.

1. Introduction

The Ediacaran-Cambrian transition witnessed a major radiation of macroscopic multicellular life including stem- and crown-group metazoans, leading to the establishment of modern-style ecosystems (Erwin et al., 2011; Wood et al., 2015; Zhu et al., 2017; Darroch et al., 2018). Although considerable effort has been put into investigating this critical interval, the patterns and causes of such biotic turnover are enigmatic and hotly debated (Darroch et al., 2023). It has been hypothesized that (a) the Cambrian biota expanded after extinction of the Ediacaran biota, potentially triggered by extreme perturbations to surface environments and global biogeochemical cycles (e.g. Amthor et al., 2003); and/or that (b) ecological engineering led to the gradual replacement of the Ediacaran biota by the Cambrian biota (e.g. Laflamme et al., 2013; Darroch et al., 2015). To test these hypotheses and to unravel the environmental controls on the rise of metazoans, it is necessary to calibrate the temporal relationship between biological evolution and environmental changes through this interval in diverse settings around the world, which hinges on the erection of a robust chronostratigraphic framework. However, such work has been hampered by a lack of fossiliferous sections that lend themselves to carbonate-based regional and global isotopic correlation (Smith et al., 2016a; Zhu et al., 2019).

The Central Iberian Zone or CIZ preserves the most complete fossiliferous Ediacaran-Cambrian successions within the Iberian Peninsula, and yields the only late Ediacaran biomineralized fossils in Europe (e.g. Vidal et al., 1994a; Cortijo et al., 2010, 2015; Zhuravlev et al., 2012), making it an ideal place to complement global correlation of the Ediacaran-Cambrian transition interval. The CIZ was located at the

* Corresponding author at: Department of Earth Sciences, University College London, WC1E 6BT, UK.
E-mail addresses: kun.zhang.19@ucl.ac.uk (K. Zhang), g.shields@ucl.ac.uk (G.A. Shields), y-zhou@ucl.ac.uk (Y. Zhou), hstrauss@uni-muenster.de (H. Strauss), ulrich.struck@mfn.berlin (U. Struck), soren@unex.es (S. Jensen).

https://doi.org/10.1016/j.precamres.2024.107526
Received 4 December 2023; Received in revised form 23 May 2024; Accepted 18 July 2024
Available online 31 July 2024

northwestern margin of Gondwana during the late Ediacaran to early Cambrian at a paleolatitude of ~40°S (Torsvik and Rehnström, 2001; Álvaro et al., 2016; Scotese, 2021). In the Ibor and Navalpino anticlines of the CIZ, *Cloudina*, *Sinotubulites*, and *Protolagena* fossils have been recovered from carbonate units of the Ibor Group, while vendotaenids and sabelliditids are common in shale interbeds of the group (Vidal et al., 1994a; Jensen et al., 2007; Cortijo et al., 2015; Álvaro et al., 2019a). *Treptichnus pedum*, the marker fossil for the Ediacaran-Cambrian boundary stratotype in Newfoundland (Brasier et al., 1994), has been reported from the upper part of the Ibor Group (Jensen and Palacios, 2016; Álvaro et al., 2019a, b). In the Valdelacasa anticline of the CIZ, *Treptichnus pedum* occurs in the lower part of the Pusa Formation, while basal olistostromes contain allochthonous *Cloudina* (Jensen et al., 2007; Cortijo et al., 2010). The underlying Cíjara Formation, stratigraphically correlative to the Ibor Group (Fig. 1), yields treptichnids in its upper part (Jensen et al., 2007). Therefore, based on the available biostratigraphy, the Ediacaran-Cambrian boundary is proposed to lie somewhere in the upper part of the Ibor Group in the Ibor and Navalpino anticlines (Álvaro

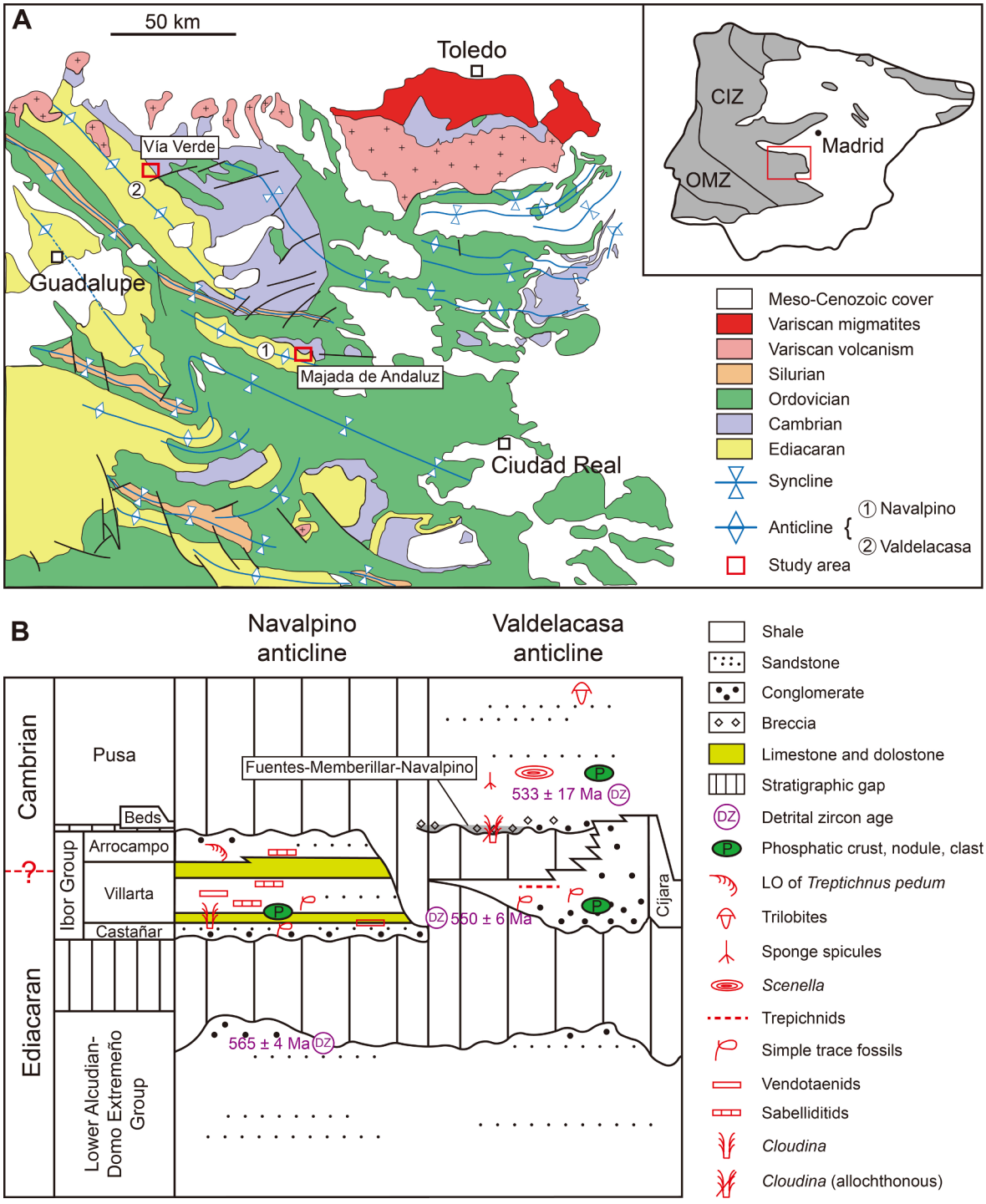

Fig. 1. (a) General geological setting in the Toledo-Alcudia Mountains, Central Iberian Zone, Iberian Peninsula (modified after Jensen and Palacios, 2016; Álvaro et al., 2020); (b) Simplified correlation of the Ediacaran-Cambrian stratigraphy in the Navalpino and Valdelacasa anticlines (modified after Álvaro et al., 2019a; Álvaro et al., 2020).

et al., 2020) and in the lower part of the Pusa Formation or the upper part of the Cíjara Formation in the Valdelacasa anticline (Jensen et al., 2007). Nevertheless, the precise placement of the boundary remains unclear due to a lack of radiometric ages and other potential markers. Although this issue has been further plagued by recent reports of co-occurrence of *Cloudina* with 'Cambrian' small shelly fossils (Yang et al., 2016; Zhu et al., 2017; Cai et al., 2019), a recent compilation of global stratigraphic data (Bowyer et al., 2022) confirms that the last appearance of *Cloudina* always underlies the first appearance of *T. pedum* in sections with high resolution carbon isotope data.

In this study, we present carbonate carbon ($\delta^{13}C_{carb}$), oxygen and strontium isotope profiles together with major and trace element data from the Villarta Formation (Ibor Group) at Majada de Andaluz in the Navalpino anticline. We also report organic carbon isotope ($\delta^{13}C_{org}$) and bulk nitrogen isotope ($\delta^{15}N$) values from the Cíjara and Pusa formations at Vía Verde in the Valdelacasa anticline. These data reveal the existence of the globally recognized basal Cambrian carbon isotope excursion (BACE) in the Central Iberian Zone. Regional correlation allows us to directly relate the BACE excursion to biotic turnover from typically Ediacaran- to Cambrian-type biota across the Ediacaran-Cambrian transition in Spain.

2. Geological setting

The Ediacaran to Cambrian strata of the Iberian Peninsula were deposited in the Cadomian retro-arc basin, which resulted from the collision of the Cadomian Arc with Gondwana (Álvaro et al., 2020). These strata in the Toledo-Alcudia Mountains of the CIZ are mainly preserved in NW-SE trending fold belts (Fig. 1). An updated and detailed Ediacaran-Cambrian stratigraphic framework in the Toledo-Alcudia Mountains is reported in Álvaro et al. (2019a). The Villarta Formation at the Majada de Andaluz section in the Navalpino anticline can be subdivided into three members (Álvaro et al., 2019a). The lower member is characterized by depositional cycles of shale-marlstone-limestone with a total thickness of ~180 m; *Cloudina* fossils are embedded within thromboid-textured limestone (Álvaro et al., 2020). The middle member is ~10 m thick and composed of conglomerates, sandstones, and shale beds. The upper member consists of alternating shales and carbonate rocks with a thickness of ~70 m. The Villarta carbonates were deposited in a shallow carbonate platform with increasing water depth towards the NE (Vidal et al., 1994a; Cortijo et al., 2015; Álvaro et al., 2020). The maximum depositional age of the lowermost Villarta Formation has been estimated at ~555–550 Ma (Álvaro et al., 2020), based on correlation of the Ibor Group with the laterally equivalent Cíjara and Hinojosas formations elsewhere in the Central Iberian Zone (Álvaro et al., 2019a) and their youngest detrital zircon SHRIMP (sensitive high resolution ion microprobe) U–Pb ages (Talavera et al., 2012; Talavera et al., 2015).

The Cíjara and Pusa formations crop out at the Vía Verde section near the La Nava de Ricomalillo village in the Valdelacasa anticline. The Cíjara Formation, about 3500 m thick, mainly comprises conglomerates and sandstones with minor shales, and is characterized by the presence of phosphatic clasts in its upper part (Álvaro et al., 2016). Simple trace fossils and possible treptichnids have been discovered from the upper Cíjara Formation (Jensen and Palacios, 2016). The Fuentes megabreccia beds, up to 100 m thick, overlie the Cíjara Formation (Jensen et al., 2007) and comprise a mixture of heterolithic clasts (both carbonate and siliciclastic, and containing *Cloudina* shells) proposed to be sourced from previously deposited formations, representing a slope-apron deposit (Álvaro, et al., 2019b). The Pusa Formation overlying the megabreccia beds can be subdivided into three members. The lower member, about 1000 m thick, is dominated by shales with minor sandstone interbeds. The carbonaceous macrofossil *Beltanelliformis* co-occurs with *Treptichnus* in this member (Brasier et al., 1979; Jensen et al., 2006, 2007; Jensen and Palacios, 2016). The middle member contains variably phosphatic shales with a thickness of ~500 m. The upper member, up to ~550 m thick, mainly consists of shales and greywacke sandstones. *Scenella*-like small shelly fossils have been reported close to the middle-upper member transition, while siltstones in the uppermost Pusa Formation yield trilobites and archaeocyaths (Jensen et al., 2010; Liñán et al., 2020). The Cíjara and Pusa formations are considered to represent deposition across the Ediacaran-Cambrian transition interval (e.g. Cortijo et al., 2010; Álvaro et al., 2016), which is consistent with detrital zircon ages of 533 ± 17 Ma (U–Pb SHRIMP) from the Pusa Formation, 550 ± 6 Ma (U–Pb SHRIMP) from the Cijara Formation, and 565 ± 4 Ma (U–Pb LA–ICP–MS; laser ablation inductively coupled plasma mass spectrometry) from the Orellana Formation, which underlies the Cíjara Formation (Talavera et al., 2012; Linnemann et al., 2018). It has been proposed that the Cíjara Formation represents deposition in the outer platform to slope environment, while the Pusa Formation could represent a deep platform environment (Vidal et al., 1994a; Cortijo et al., 2010; Jensen and Palacios, 2016).

3. Materials and methods

Eighty-one carbonate samples were collected from the Majada de Andaluz section in 2006, and twenty-seven shale samples were collected from the Vía Verde section in 2007. Stratigraphic heights of Majada samples have been assigned by comparing original field notes with the published stratigraphic column of Álvaro et al. (2019b), further informed by field excursions in 2019 and 2022. Member/major bed assignments of all samples have been confirmed so that stratigraphic trends can be reliably correlated into the published stratigraphic framework. The Vía Verde section consists of outcrop in the trenches along an abandoned railway section that within the study area runs parallel to the Huso river. Samples were collected along approximately 10 km of section with 16 samples in the Cijara Formation and 11 samples in the Pusa Formation. Precise stratigraphic placement of samples within the Cijara Formation is not possible because of covered areas in a section with some structural complexity (e.g. Vidal et al., 1994b). Progressively higher positions northwards are however evident.

Thin sections of the carbonate samples from the Majada section were scrutinized under a polarizing microscope in order to identify the best-preserved rock components destined for element and isotope analyses. The powders were then drilled on the counterpart of the rock slabs while avoiding visible alteration, such as calcitic micro-veins and interstitial cements. CO_2 for carbon and oxygen isotope analyses was liberated from whole rock carbonates via off-line phosphorylation (cf. McCrea, 1950) with enriched phosphoric acid (Wachter and Hayes, 1985) at 50 °C for 24 h (limestone) or 48 h (dolomite) and subsequent cryogenic distillation. All carbonate carbon and oxygen isotope analyses were carried out at the Institut für Geologie und Paläontologie in Münster, Germany, using a Thermo Finnigan Delta Plus mass spectrometer. Results are reported in the standard delta notation as $\delta^{13}C$ and $\delta^{18}O$ relative to VPDB (Vienna Pee Dee Belemnitella). Standard deviation, as determined from replicate analyses, was usually better than 0.15‰ and 0.2‰ for carbon and oxygen isotopes, respectively.

Another aliquot of the carbonate sample powders from the Majada section was leached by excess 10% hydrochloric acid at room temperature for at least 12 h. The concentrations of some diagnostic major and trace elements (Ca, Mg, Fe, Mn and Sr) were determined using ICP-AES (inductively coupled plasma atomic emission spectroscopy) at the Wolfson Laboratory of University College London in 2010. The precisions are generally better than 5% for the analysed elements based on long-term reproducibility of laboratory measurements of standard reference materials.

A small number of samples (five limestones and one dolostone) from the Majada section were then selected for Sr isotope stratigraphy (SIS) study following strict petrographic and geochemical selection criteria. Limestone samples with high Sr and carbonate contents, low Mn/Sr ratios and plausible O-isotopes were selected, whereby only primary rock components were then micro-drilled. Only one dolomitic sample

was run for comparison. A sequential leaching method was employed to prepare them for Sr isotope analysis. Fine powders of the samples were pre-leached by 0.13 M acetic acid using a volume calculated to dissolve around one-third of the carbonate fraction, aiming to remove silicate-related contaminants and altered carbonate components, before dissolving another ~40 % using the same acetic acid for SIS study. Sr was eluted from solutions with any remaining Rb eliminated through ion exchange column chromatography. Sr isotope values were determined using thermal ionization mass spectrometry (TIMS; Phoenix Isotopx) at Royal Holloway, University of London, with $^{87}Sr/^{86}Sr$ of the standard reference material NBS 987 at 0.710240 ± 0.000008 (mean and 2SE, N=13).

For the shale samples from the Vía Verde section, organic carbon and bulk nitrogen concentration and isotope analyses were both performed at the laboratories of the Museum für Naturkunde, Berlin in 2008 using a Thermo Finnigan Flash Elemental Analyser 1112 coupled to a Thermo Delta V Mass Spectrometer (continuous flow). After washing, samples were cut into small chips for powdering. For bulk rock samples, the amount of powder required for a detectable amount of nitrogen ranged between 10 mg and 200 mg depending on clay and/or organic content. The natural drift observed for the reference has been used to correct the samples' values. All the results characterized by a TN content below 0.020 μg (accuracy limit for our analytical setup) have been measured at least twice to demonstrate their fidelity. The final analytical errors for both $\delta^{15}N$ and $\delta^{13}C$ analyses amount to no greater than ±0.5‰.

4. Results

4.1. Majada de Andaluz section

For the lower member of the Villarta Formation, the carbonate samples are dominated by limestones in its lower part with Mg/Ca ratios generally lower than 0.06, while carbonates in its upper part are dominated by dolostones characterized by high Mg/Ca ratios ranging within 0.4–0.5 (Fig. 2). The limestones in the lower part are enriched in Sr averaging 2145 ppm, yet the dolostones in the upper part are depleted in Sr averaging 39 ppm. Similarly, the Mn/Sr ratios are generally lower than 1.0 but higher than 100 in the limestones (lower part) and dolostones (upper part), respectively (Fig. 2). There are only few carbonate beds in the middle member where the Mg/Ca ratios are greater than 0.06. In the upper member, the Mg/Ca ratios exhibit great variability ranging between 0.01 and 0.46 whereas the corresponding Mn/Sr ratios are generally lower than 10 (Fig. 2). The Sr concentrations show relatively small differences among samples that have been dolomitized to varying extents (Fig. 2). Specifically, the average Sr concentrations are 620 ppm and 213 ppm for limestones (Mg/Ca < 0.06) and dolomitized samples (Mg/Ca > 0.06), respectively, in the upper member.

The $\delta^{13}C_{carb}$ values of the lower member show a gradually increasing trend from −2.5‰ to +2.7‰, largely stabilize between +1‰ and +3‰ in its lower part, followed by a shift to −2‰ in its upper part accompanied by the lithological change from limestone to dolostone (Fig. 2). A pronounced negative carbon isotope excursion with values as low as −8.4‰ is revealed within a carbonate band in the upper part (Fig. 2). In the middle to upper member of the Villarta Formation, the $\delta^{13}C_{carb}$ record is characterized by a negative plateau mainly ranging around −3‰. The $\delta^{18}O$ values of the lower member mainly range between −10‰ and −14‰ in its lower part (limestone) and between −6‰ and −8‰ in its upper part (dolostone). The middle to upper member is characterized by scattered $\delta^{18}O$ values ranging between −6‰ and −15‰ with an average value of −12‰. The $^{87}Sr/^{86}Sr$ ratios of limestone samples range between 0.708512 and 0.708838, whereas the dolostone sample has a significantly higher ratio of 0.711685 (Fig. 2).

4.2. Vía Verde section

At Vía Verde, the lithology changes from mainly sandstone in the the Cíjara Formation to shale in the Pusa Formation. The shale samples from the Cíjara Formation are characterized by $\delta^{13}C_{org}$ values of around −27‰ to −25‰, but with one prominent negative value of −35.6‰ in its middle-upper part (VJ11, see supplementary figure for sample location). The shale samples from the overlying Pusa Formation exhibit systematically lower $\delta^{13}C_{org}$ values between −30‰ and −28‰ (Fig. 3).

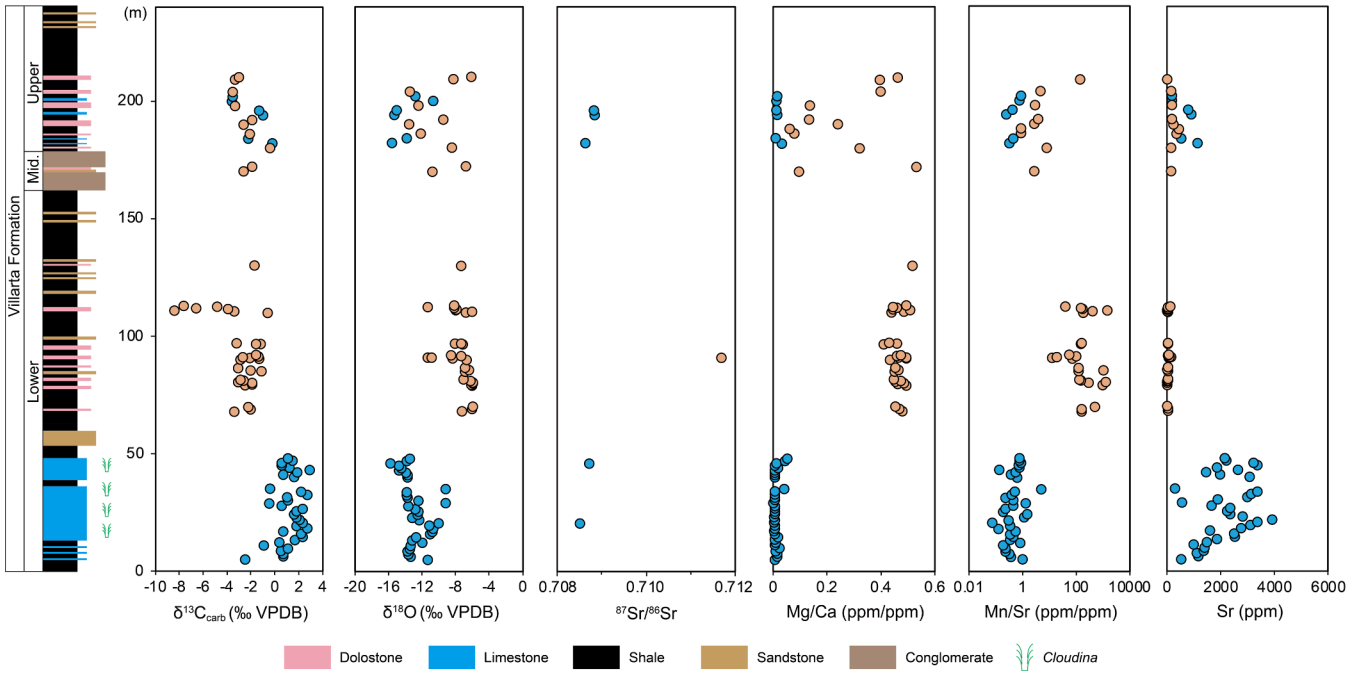

Fig. 2. Chemostratigraphic profiles of $\delta^{13}C_{carb}$, $\delta^{18}O$, $^{87}Sr/^{86}Sr$, Mg/Ca, Mn/Sr ratios and Sr concentrations for the Villarta Formation at the Majada section, Spain. Blue circles represent limestones with Mg/Ca ratios < 0.06 while orange circles represent samples of varying degrees of dolomitization with Mg/Ca ratios > 0.06. The stratigraphic column is modified after Álvaro et al. (2019b).

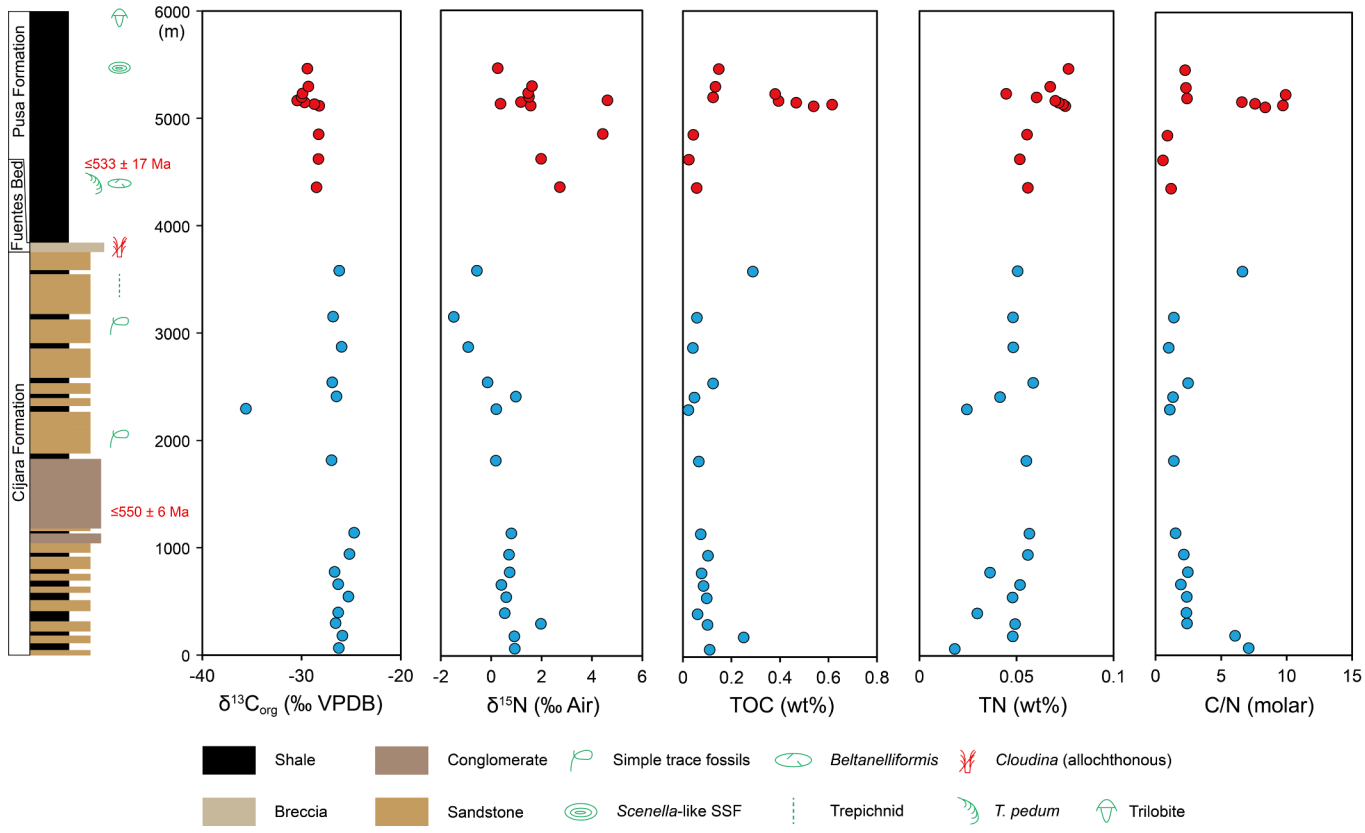

Fig. 3. Chemostratigraphic profiles of $\delta^{13}C_{org}$, $\delta^{15}N$, TOC, TN, and C/N for the Cíjara and Pusa formations at the Vía Verde section, Spain. Blue circles represent Cíjara Formation samples and red circles represent Pusa Formation samples. Fossil occurrences are based on Jensen and Palacios (2016) and Álvaro et al. (2020). Age constraints are based on Talavera et al. (2012). The stratigraphic column is modified after Álvaro et al. (2019b).

The $\delta^{15}N$ values show a decreasing trend from +0.94‰ to −1.49‰ (mean +0.37‰) through the Cíjara Formation, but fluctuate significantly within a range between +0.26‰ and +4.62‰, with a higher average value of +1.98‰, in the Pusa Formation (Fig. 3). The TOC contents are generally low at the Vía Verde section, ranging from 0.02% to 0.28% (average 0.10%) in the Cíjara Formation and from 0.02% to 0.61% (average 0.27%) in the Pusa Formation (Fig. 3). The TN values show a broadly increasing trend from 0.018% to 0.077% upward with average values of 0.045% in the Cíjara Formation and 0.064% in the Pusa Formation (Fig. 3). The C/N molar ratios are in the range of 0.6–9.9 (average 3.5; Fig. 3).

5. Discussion

5.1. Diagenetic evaluation

5.1.1. Majada de Andaluz section

Diagenetic processes that alter the isotopic and elemental compositions of carbonate rocks can mask the primary values and/or trends. It is therefore important to evaluate the effects of diagenesis before chemostratigraphic correlation can be attempted. In addition to petrographic observation, the most commonly used geochemical indicators for diagenetic screening include Sr concentrations, Mn/Sr ratios and $\delta^{18}O$ values (e.g. Kaufman and Knoll, 1995). This is because these elements and isotopic values can be altered at relatively low fluid/rock ratios and thus are very sensitive to diagenesis (Brand and Veizer, 1980; Banner and Hanson, 1990). However, the resistance of different proxies to diagenesis is variable, and the same proxy could exhibit different behaviour under different ambient fluid conditions (e.g. Lau and Hardisty, 2022; Zhang and Shields, 2023). This means that the alteration of sensitive proxies does not necessarily indicate any distortion of systems less prone to diagenesis, such as carbon isotopes. Nevertheless, these sensitive indicators provide a simple and straightforward way to constrain the extent of diagenetic alteration and therefore have been widely applied in chemostratigraphic studies (e.g. Brasier et al., 1996; Bartley et al., 1998; Li et al., 2013; Kuznetsov et al., 2017).

Progressive diagenetic exchange generally leads to Mn enrichment and Sr depletion in carbonate rocks, along with a decrease in both $\delta^{13}C_{carb}$ and $\delta^{18}O$ values (Brand and Veizer, 1980; Bartley et al., 1998). Carbonate rocks with oxygen isotope values lower than −10‰ are commonly considered to have been altered (Kaufman and Knoll, 1995). At first glance, geochemical data in the lower member could be taken to imply that there has been significant diagenetic alteration and elemental mobilization. For the lower part of the lower member, such low $\delta^{18}O$ values (mostly < −10‰) could indicate that samples underwent significant isotopic exchange with meteoric and/or higher temperature fluids. However, the lower part is also characterized by low Mg/Ca (<0.06), low Mn/Sr (mostly < 1), high Sr contents (Fig. 2), and $^{87}Sr/^{86}Sr$ ratio of 0.708512 (Fig. 2) that is consistent with the coeval seawater value (Zhou et al., 2020; McArthur et al., 2020). The preservation of primary seawater $^{87}Sr/^{86}Sr$ ratios suggests that the diagenetic system was relatively closed. Considering their high Sr contents (up to 3917 ppm), one possible explanation for the low $\delta^{18}O$ values is that carbonate rocks of the lower part were originally composed of aragonite that was replaced during burial diagenesis under low water/rock ratios (cf. Tucker, 1986). The absence of significant correlation between $\delta^{13}C_{carb}$ and $\delta^{18}O$ and other parameters in lower carbonates also argues against significant diagenetic alteration of carbon isotopes (Fig. 4).

In the upper part of the lower member, accompanied by increased Mg/Ca ratios, indicating partial dolomitization, Mn/Sr ratios increase dramatically from ~1 to ~100, while Sr is significantly depleted (Fig. 2). Although the Mn/Sr ratio is also redox controlled (e.g. Shields et al.,

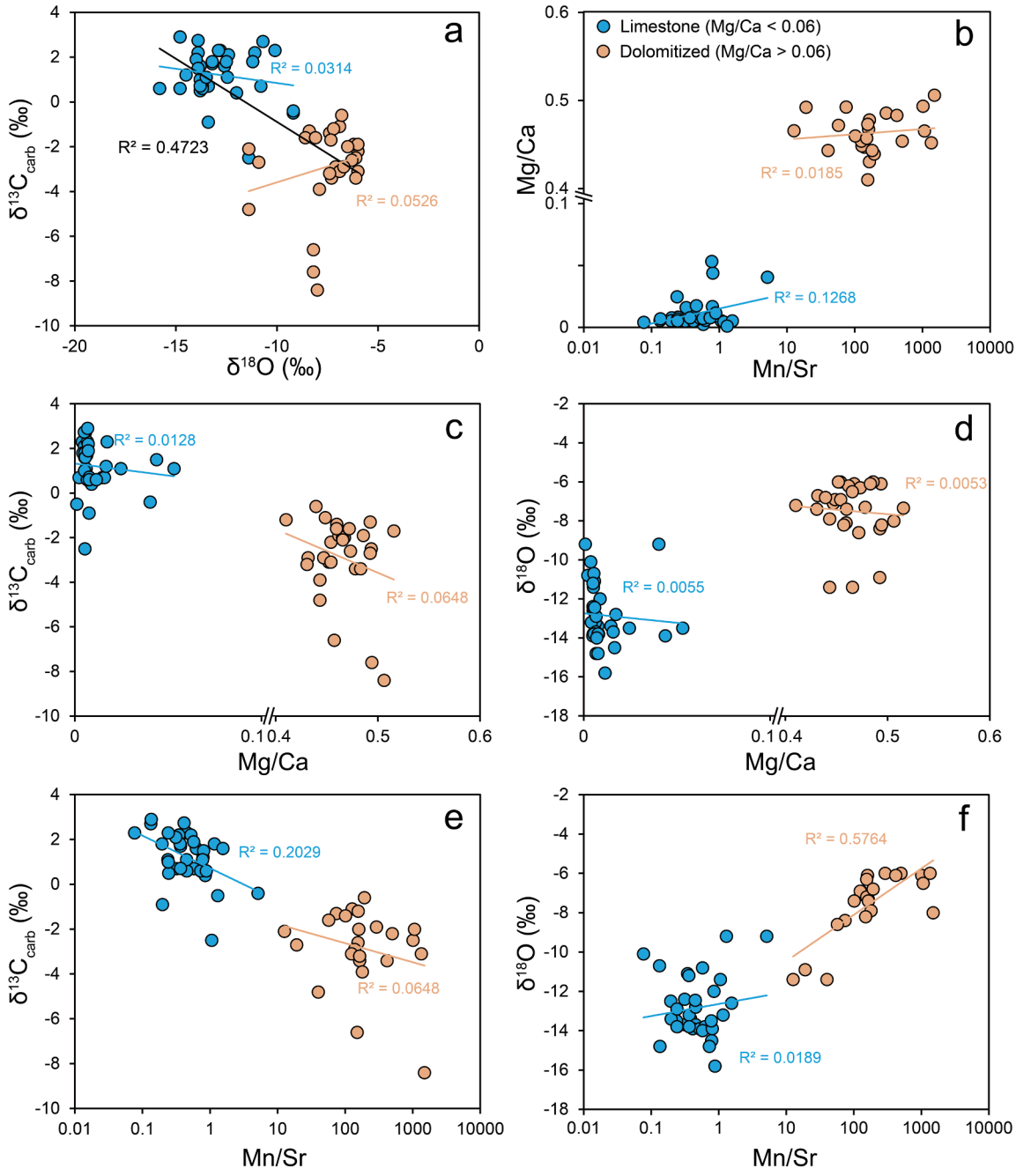

Fig. 4. Cross plots of (a) $\delta^{13}C_{carb}$ vs. $\delta^{18}O$, (b) Mg/Ca vs. Mn/Sr, (c) $\delta^{13}C_{carb}$ vs. Mg/Ca, (d) $\delta^{18}O$ vs. Mg/Ca, (e) $\delta^{13}C_{carb}$ vs. Mn/Sr, and (f) $\delta^{18}O$ vs. Mn/Sr for the lower member of the Villarta Formation at the Majada section. Blue and orange circles represent limestones (Mg/Ca < 0.06) and dolomitized samples (Mg/Ca > 0.06), respectively. The black line in (a) represents the trendline of all samples from the lower member.

1997; Ossa Ossa et al., 2018), we consider its substantial range to relate to the loss of Sr during diagenesis. Since Sr preferentially substitutes for Ca in the crystal lattice, its concentration may decrease with increasing dolomitization (Vahrenkamp and Swart, 1990). Therefore, simultaneous covariation between Mg/Ca, Mn/Sr and Sr/Ca is most parsimoniously interpreted as the result of significant dolomitization. Moreover, $\delta^{18}O$ values of the upper part are more positive compared to the lower part, which also likely reflects the minerology change. It is generally accepted that dolomite in isotopic equilibrium with calcite is enriched in ^{18}O by about 3–6‰ (see review in Swart, 2015). If an isotopic offset of 6‰ is applied, $\delta^{18}O$ values of the upper part are consistent with the measured range of the lower part. Taken together, the elemental and oxygen isotopic changes from the lower to upper part of the lower member can be attributed to dolomitization.

The relationship between dolomitization and carbon isotopes is more ambiguous. Laboratory precipitation experiments suggest that dolomite is enriched in ^{13}C by 1–2‰ relative to calcite (Horita, 2014), while many Precambrian dolomites are believed to precipitate during early marine diagenesis and thus preserve seawater carbon isotope composition (e.g. Hood et al., 2018). In addition, since dolomitization is often associated with organic matter decomposition, which will produce ^{12}C-enriched fluids, dolomites may therefore have more negative $\delta^{13}C_{carb}$ values (e.g. Kaufman and Knoll, 1995). For instance, it has been reported that dolomitization can produce significantly lower values of $\delta^{13}C_{carb}$ in dolostones than that in the coeval limestones (e.g. Bold et al., 2020; Nelson et al., 2021). The most distinctive feature in the upper part of the

lower member is the pronounced negative $\delta^{13}C_{carb}$ excursion to values as low as −8.4‰. Although the robustness of these low values can be questioned because oxygen isotopes and elemental indices suggest a greater extent of alteration compared with the lower part, comparable $\delta^{13}C_{carb}$ values in both limestones and dolomitized samples higher in the succession (Fig. 2) lend some credence that these values have not been significantly reset. The absence of covariation between Mg/Ca, Mn/Sr, $\delta^{18}O$ and $\delta^{13}C_{carb}$ values in upper part samples also suggests that the $\delta^{13}C_{carb}$ stratigraphic trends have not been biased by diagenesis. Notably, although a positive correlation between $\delta^{13}C_{carb}$ and $\delta^{18}O$, as generally expected in diagenetic carbonates, is not observed, there is indeed a weak negative covariation between the two parameters within the lower member as a whole (Fig. 4), which has also been reported by Álvaro et al. (2020). Considering the opposite effects of diagenesis on $\delta^{18}O$ in the lower and upper parts, such a negative covariation might simply be induced by $\delta^{18}O$ variability that is not indicative of systematic $\delta^{13}C_{carb}$ alteration. This observation echoes the previous argument that the use of $\delta^{18}O$ for diagenetic screening becomes more ambiguous when different diagenetic processes, especially dolomitization, occur (e.g. Li et al., 2013).

For the middle to upper members of the Villarta Formation, which have been dolomitized to different degrees, the dolomitized samples appear to have less negative $\delta^{18}O$ values, higher Mn/Sr ratios and lower Sr concentrations compared to limestone samples (Fig. 2). It is thus also possible that, as discussed above, most of the elemental and oxygen isotopic variability was induced by dolomitization. The weak positive

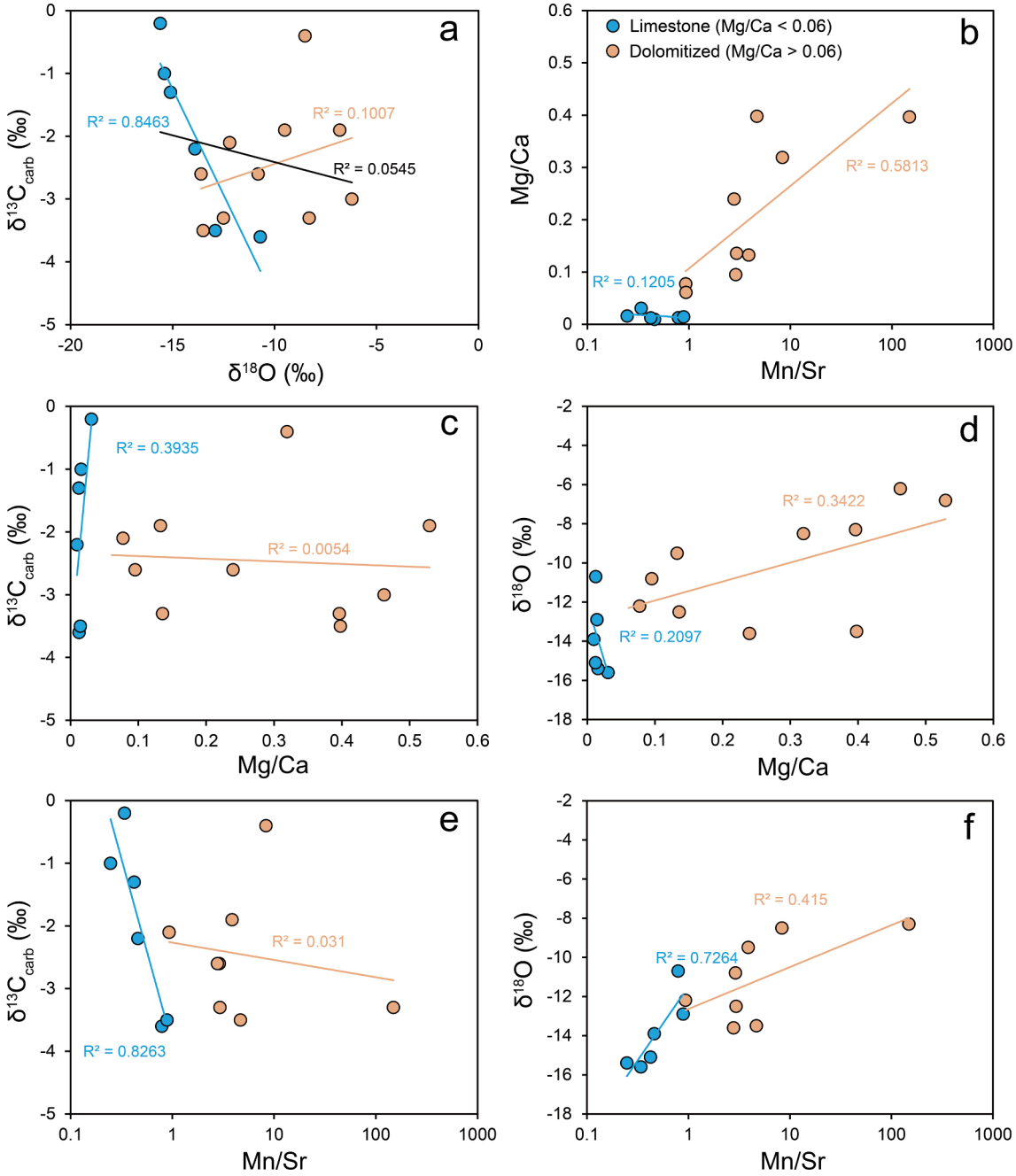

Fig. 5. Cross plots of (a) $\delta^{13}C_{carb}$ vs. $\delta^{18}O$, (b) Mg/Ca vs. Mn/Sr, (c) $\delta^{13}C_{carb}$ vs. Mg/Ca, (d) $\delta^{18}O$ vs. Mg/Ca, (e) $\delta^{13}C_{carb}$ vs. Mn/Sr, and (f) $\delta^{18}O$ vs. Mn/Sr for the middle to upper member of the Villarta Formation at the Majada section. Blue and orange circles represent limestones (Mg/Ca < 0.06) and dolomitized samples (Mg/Ca > 0.06), respectively. The black line in (a) represents the trendline of all samples from the middle to upper member, irrespective of mineralogy.

covariations among diagenetic indicators in the dolomitized samples (Fig. 5) provide further support for the inference that dolomitization has led to Sr loss and ^{18}O enrichment. The limestones in the upper member are characterised by high Sr concentrations (up to 1139 ppm) and low $\delta^{18}O$ values (<−10‰). Similar to the lower part of the lower member, the low $\delta^{18}O$ values can be attributed to burial diagenesis (Tucker, 1986). Interestingly, Mn/Sr, $\delta^{18}O$ and $\delta^{13}C_{carb}$ exhibit strong negative covariations in the limestones (Fig. 5). However, one would expect the opposite (i.e. positive correlation between $\delta^{18}O$ and $\delta^{13}C_{carb}$), had burial diagenesis reset the carbon isotope compositions (Derry, 2010). Considering the consistently low Mg/Ca (<0.06) and Mn/Sr (<1) ratios, we therefore interpret the covariations to correspond to primary stratigraphic trends, indicating that the $\delta^{13}C_{carb}$ values of limestones have not been significantly altered. In addition, dolomitized samples show neither strong covariation between $\delta^{18}O$, Mg/Ca, Mn/Sr and $\delta^{13}C_{carb}$ (Fig. 5), nor remarkably different $\delta^{13}C_{carb}$ values from limestones from the same stratigraphic level (Fig. 2). Therefore, $\delta^{13}C_{carb}$ values of dolomitized samples appear little modified. In conclusion, although carbonate rocks in the Villarta Formation at the Majada section have been altered by diagenetic processes, we suggest that the carbon isotope values have not been significantly altered for the purpose of chemostratigraphic correlation.

The $^{87}Sr/^{86}Sr$ ratios of carbonate rocks are prone to diagenesis, and therefore screening is generally applied in SIS studies, including this study (see Methods), whereby the most evidently altered samples have not been selected for isotopic analysis. The chosen limestone samples have high Sr concentrations (792–3365 ppm), low Mn/Sr ratios (0.08–0.88) and low Fe/Sr ratios (1.08–4.20), which satisfy most

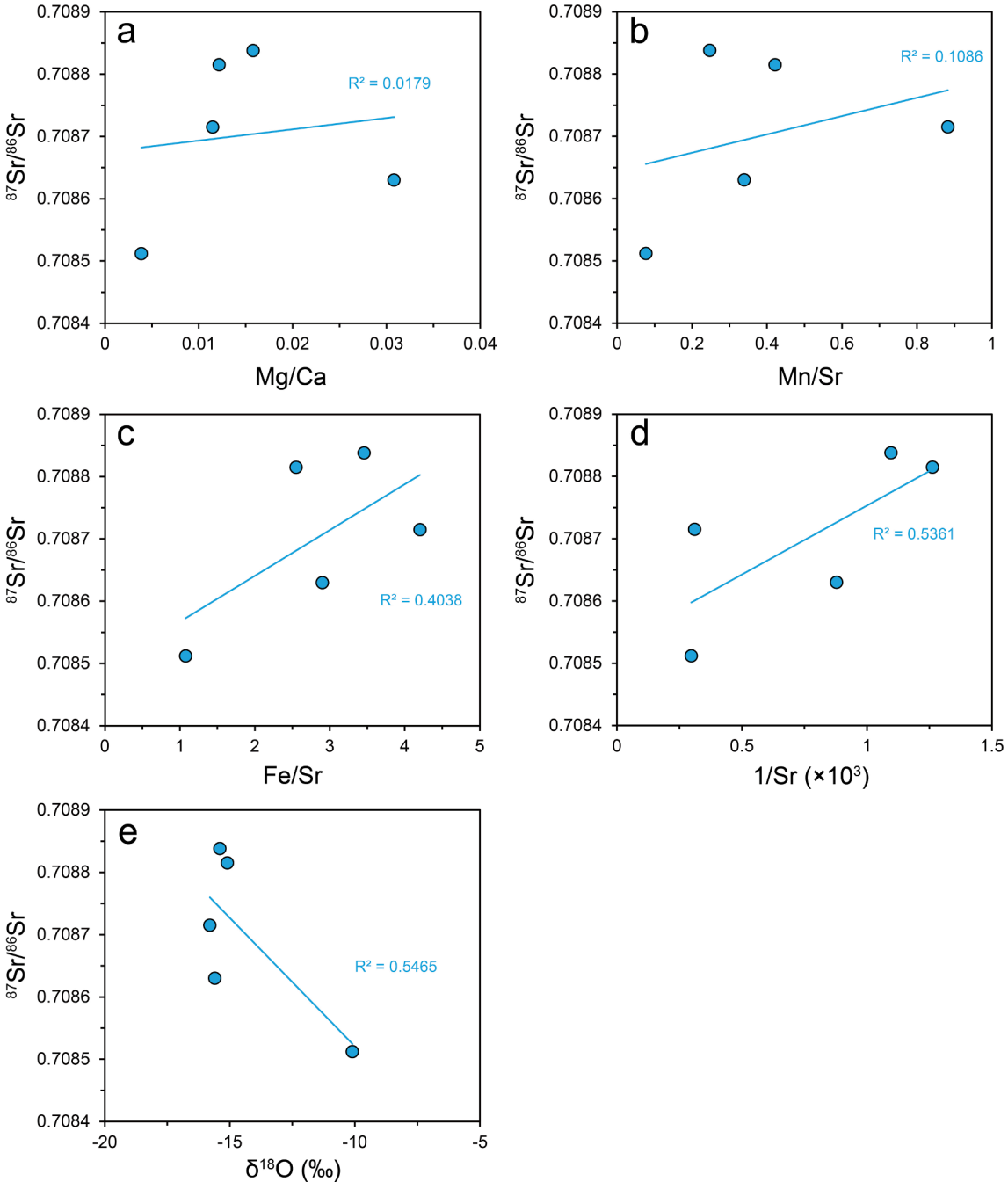

Fig. 6. Cross plots of $^{87}Sr/^{86}Sr$ ratios against Mg/Ca (a), Mn/Sr (b), Fe/Sr (c), 1/Sr ratios (d) and $\delta^{18}O$ values (e) for the limestones in the Villarta Formation at the Majada section.

screening criteria in the literature (see a recent review in X. Chen et al., 2022). No significant covariations between Mg/Ca, Mn/Sr and $^{87}Sr/^{86}Sr$ ratios in limestones are evident. Although their Sr isotope values appear to covary slightly with Fe/Sr ratios, Sr concentrations and $\delta^{18}O$ values (Fig. 6), it remains unclear whether it truly reflects alteration given the limited number of data points. During the Ediacaran-Cambrian transition, the contemporaneous seawater Sr isotope values likely stabilized at ~0.7085, but do show a certain variability (see Bowyer et al. (2022) for a compilation). From a conservative view, we consider that the lowest $^{87}Sr/^{86}Sr$ value (0.708512) represents the most pristine value and thus likely seawater value, yet other $^{87}Sr/^{86}Sr$ values (0.708630–0.708838) may have been slightly altered. On the other hand, the dolostone sample is characterized by high Mn/Sr (19.14) and Fe/Sr (233.14) ratios, low Sr concentration (81 ppm) and a markedly higher $^{87}Sr/^{86}Sr$ ratio (0.711685) than for coeval seawater (Zhou et al., 2020; X. Chen et al., 2022), and is likely to have been significantly altered.

5.1.2. *Vía Verde section*

Depending on the openness of a rock system, ammonium that is transformed from organic-bound nitrogen, either through organic remineralisation during early diagenesis or thermal maturation of organic matter, can be captured by clay minerals or lost from the system. $\delta^{15}N$ can be a reliable proxy only when the signal is unaltered by post-depositional processes (Mettam and Zerkle, 2021). At Vía Verde, there is no significant covariation between TN and TOC but with a non-zero y-axis intercept for the Cíjara and Pusa samples (Fig. 7a), suggesting the existence of both organic- and clay-bound nitrogen. Although

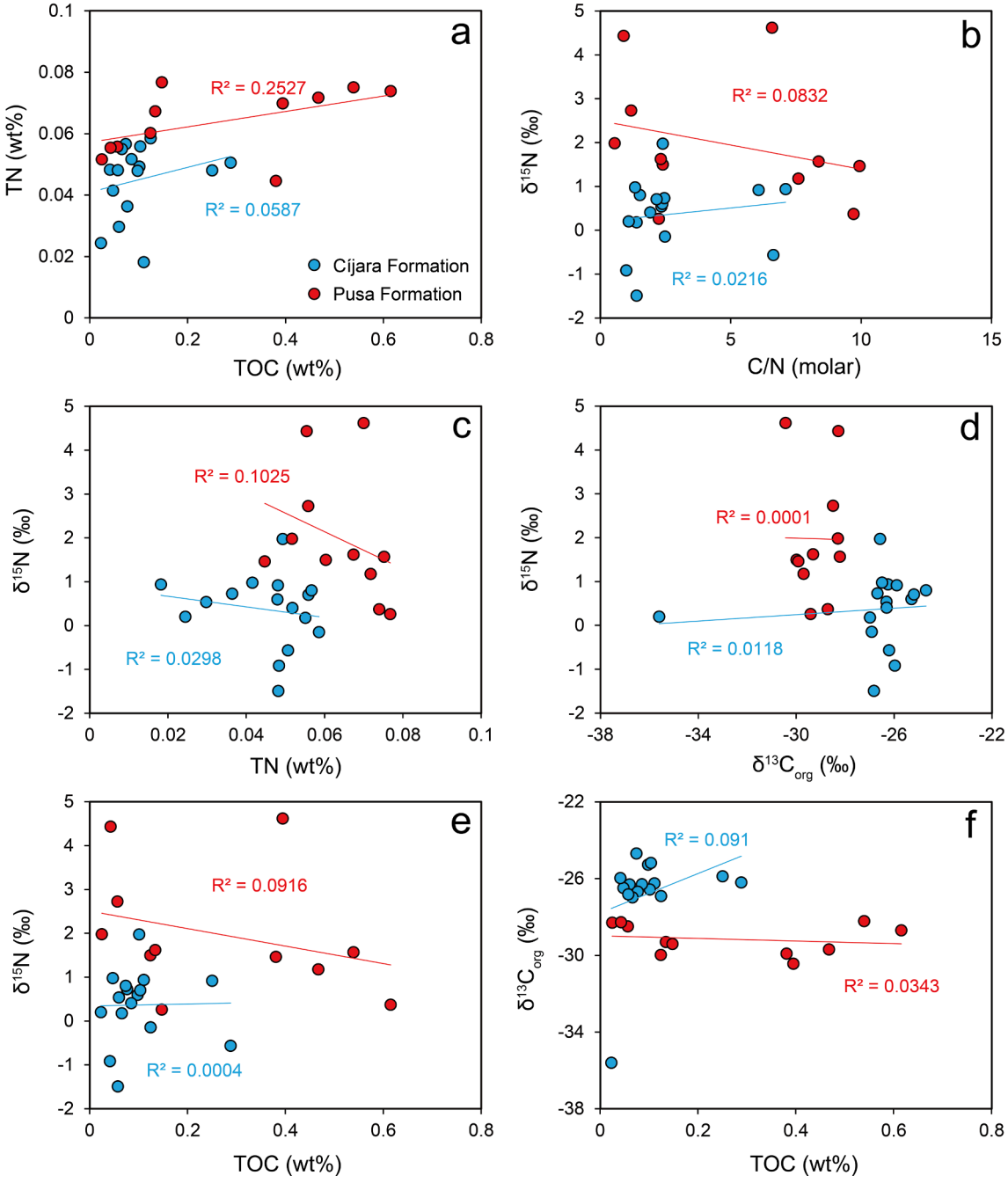

Fig. 7. Cross plots of (a) TN vs. TOC, (b) $\delta^{15}N$ vs. C/N, (c) $\delta^{15}N$ vs. TN, (d) $\delta^{15}N$ vs. $\delta^{13}C_{org}$, (e) $\delta^{15}N$ vs. TOC, and (f) $\delta^{13}C_{org}$ vs. TOC in the Cíjara Formation (bule circles) and the Pusa Formation (red circles) at the Vía Verde section, Spain.

preferential loss of ^{14}N due to organic matter degradation during early diagenesis can increase $\delta^{15}N$ values by as much as 4‰ (Freudenthal et al., 2001), the generally low C/N ratios in the Cíjara Formation (mean 2.7) and the Pusa Formation (mean 4.7) indicate that liberated NH_4^+ was largely incorporated into clay minerals (Mettam and Zerkle, 2021), suggesting minimal influence of early diagenesis on measured $\delta^{15}N$ values (Stüeken et al., 2016). Allochthonous nitrogen from detrital minerals (e.g. due to the lithological change) may also cause low C/N ratios, whereby significant covariation between C/N, TN, and $\delta^{15}N$ would be expected. However, $\delta^{15}N$ data show no covariation between C/N and TN in both the Cíjara and Pusa formations (Fig. 7b, c), implying only a limited impact of allochthonous nitrogen on $\delta^{15}N$ values.

Thermal alteration during thermal maturation and/or metamorphism generally leads to preferential removal of lighter stable isotopes (i.e. ^{12}C and ^{14}N), which produces diagnostic covariation between $\delta^{15}N$ and TN, $\delta^{15}N$ and $\delta^{13}C_{org}$, $\delta^{15}N$ and TOC, $\delta^{13}C_{org}$ and TOC in altered rocks (e.g. Mettam et al., 2019). However, no obvious covariation has been observed among those parameters in either the Cíjara or Pusa formations (Fig. 7c-f). Taken together, our data suggest insignificant post-depositional alteration of $\delta^{13}C_{org}$ and $\delta^{15}N$ values, which likely represent primary signatures.

5.2. The BACE excursion correlation

5.2.1. Regional correlation

Despite advances in biostratigraphic correlation of the Ediacaran-Cambrian boundary in Spain (Jensen et al., 2007; Cortijo et al., 2015; Jensen and Palacios, 2016; Álvaro et al., 2019a), the BACE excursion has not been explicitly identified in the Toledo-Alcudia Mountains area. Since multiple transient negative $\delta^{13}C_{carb}$ excursions have been identified during the late Ediacaran to early Cambrian interval (Nelson et al., 2023; Bowyer et al., 2023), any identification of BACE requires caution.

The maximum depositional age of the Villarta Formation has been previously constrained at about 555–550 Ma by correlation with laterally equivalent formations (Álvaro et al., 2020), which is in agreement with a recently reported maximum depositional age of 560 ± 2 Ma from the underlying Castañar Formation using U-Pb chemical abrasion-isotope dilution-thermal ionization mass spectrometry (CA-ID-TIMS) on tuffite zircons (Álvaro et al., 2024). At Majada, the well-preserved limestones near the base of the section document a rise in $\delta^{13}C_{carb}$ values from negative (−2.5‰) to low positive values (+2.7‰), which is associated with the appearance of *Cloudina* and a pristine Sr isotope value of 0.708512 (Fig. 2). Such a temporal pattern resembles closely a recently recognized negative $\delta^{13}C_{carb}$ excursion in strata from Namibia (e.g. Bowyer et al., 2022) and South China that is dated at ca. 550 Ma (Bowring et al., 2007; Yang et al., 2021). This similarity provides support for the above maximum depositional age for the Villarta Formation (Álvaro et al., 2020), but does not exclude the possibility for an even younger age for the base of the Villarta Formation, considering that the emerging global stratigraphic framework of the late Ediacaran is still evolving (Bowyer et al., 2022; Bowyer et al., 2023). Trace fossils with sediment penetration depth around 7 mm in the upper member of Villarta Formation at Majada have been interpreted to imply an earliest Cambrian age (Álvaro et al., 2020). Although *Treptichnus pedum* has so

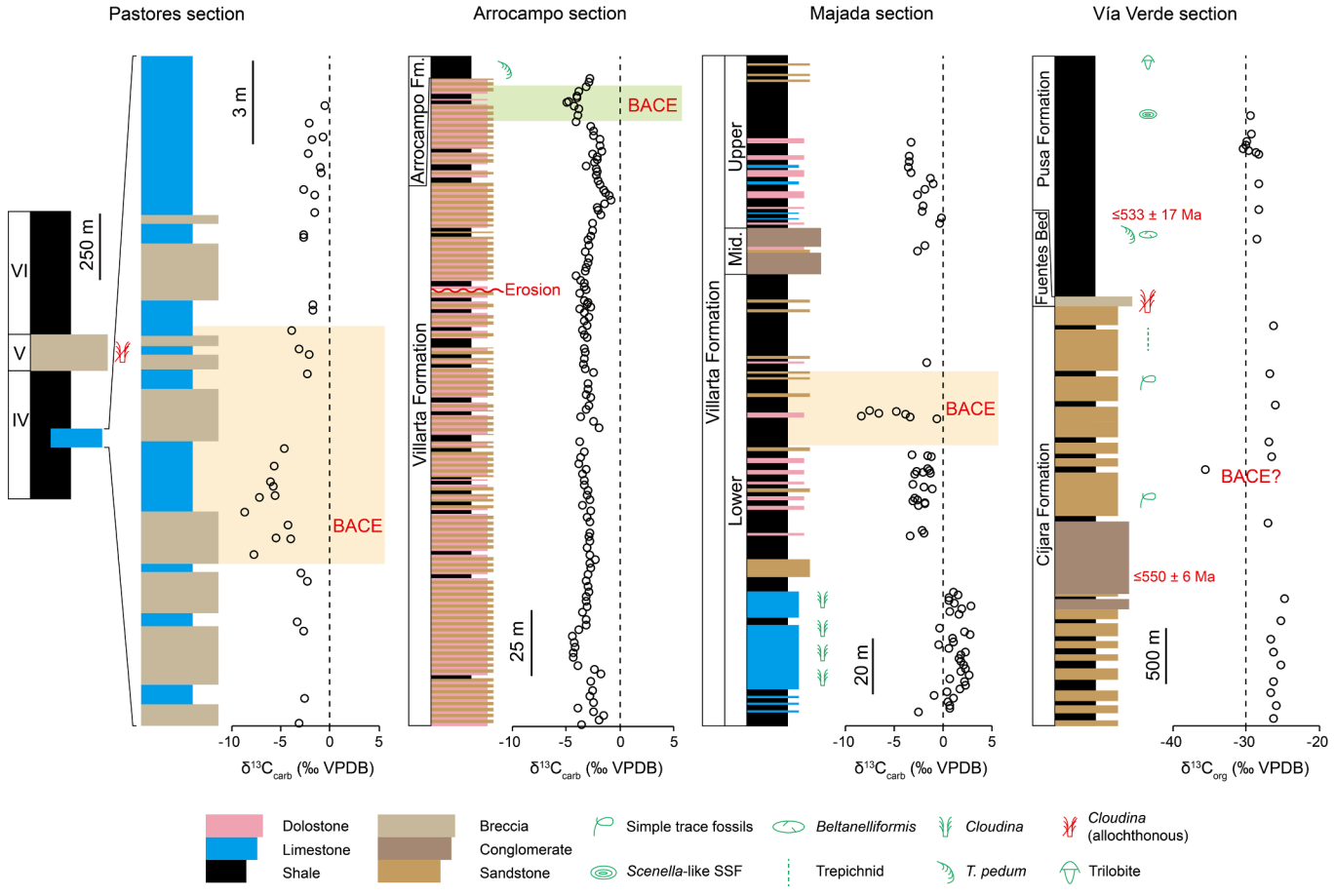

Fig. 8. Regional carbon isotope stratigraphic correlation across the Ediacaran-Cambrian transition in the Central Iberian Zone. The Pastores section is modified after Valladares et al. (2006). The Arrocampo section is modified after Álvaro et al. (2024). Light green and orange represent possible positions for the BACE based on Álvaro et al. (2024) and this study, respectively. Note that *Cloudina* found above the BACE at Pastores and Vía Verde is of allochthonous origin derived from previously deposited formations (Valladares et al., 2006; Álvaro et al., 2019a).

far not been observed in the Villarta Formation at Majada, it has been found close to the base of the overlying Arrocampo Formation at a nearby section (the Arrocampo type area; Jensen and Palacios, 2016). In conjunction with the presence of *Cloudina*, *Sinotubulites*, and *Protolagena* in the Villarta Formation (Cortijo et al., 2015), it strongly indicates that the two formations straddle the Ediacaran-Cambrian boundary (Álvaro et al., 2020).

Recently, Álvaro et al. (2024) propose that the negative shift of $\delta^{13}C_{carb}$ to −5.0‰ in the uppermost part of the Villarta Formation at Arrocampo potentially corresponds to the BACE (Fig. 8). BACE identification at Arrocampo is potentially ambiguous because $\delta^{13}C_{carb}$ values mostly stabilize at around −3‰ there, while a similar negative $\delta^{13}C_{carb}$ shift from −1.5‰ to −4.4‰ occurs near the bottom of the section (Álvaro et al., 2024). Moreover, the pattern of negative $\delta^{13}C_{carb}$ values interrupted by short-lived positive $\delta^{13}C_{carb}$ excursions at Arrocampo resembles more closely the Fortunian Stage than the late Ediacaran (Bowyer et al., 2023).

The correlation of the Villarta Formation between Majada and Arrocampo areas remains contentious, and it should be noted that the Villarta Formation is composed of dolostone at Arrocampo but comprises limestones in its lower member at Majada. Nevertheless, the negative $\delta^{13}C_{carb}$ excursion identified in the lower member of the Villarta Formation at Majada offers an alternative stratigraphic level for the BACE (Fig. 8). A similarly positive $\delta^{13}C_{carb}$ excursion to −0.2‰ followed by a swing to more negative values is exhibited near the top of the Villarta Formation at Majada (Fig. 2), suggesting that the top of the formation can be correlated between the two areas. If the BACE is situated in the lower member of the Villarta Formation, the strata at Arrocampo might thus only record the upper part of the formation. Consequently, the positive $\delta^{13}C_{carb}$ shift near the top may correspond to 2p or 3p (nomenclature from Bowyer et al. 2023), implying that the first occurrence of *T. pedum* postdates the positive excursions. If the BACE occurs in the uppermost part of the Villarta Formation, then the relatively stable negative $\delta^{13}C_{carb}$ plateau likely corresponds to a similar, short-lived negative plateau that precedes the BACE in Laurentia (Nelson et al., 2023), Mongolia (Smith et al., 2016b; Topper et al., 2022), and Siberia (Bowyer et al., 2023), implying a significantly higher sedimentation rate at Arrocampo. As such, the model of Álvaro et al. (2024) likely places the first occurrence of *T. pedum* just after the BACE and well before the 2p excursion peak. Although both models require more testing, we note that *T. pedum* mostly occurs no earlier than peak 2p in successions where both *T. pedum* and the BACE have been identified (Bowyer et al., 2023).

The Cíjara Formation is correlated with the Ibor Group in the Toledo-Alcudia Mountains, and its age has been constrained to latest Ediacaran based on published detrital zircon ages (Talavera et al., 2012; Linnemann et al., 2018). At Vía Verde, the Cíjara Formation, dominated by siliciclastic sediments, mostly has $\delta^{13}C_{org}$ values of around −26‰. The most prominent feature is that it contains a significantly lower value of −35.6‰ in its middle-upper part, stratigraphically below occurrences of treptichnids and *Treptichnus pedum* (within the Pusa Formation). Allochthonous *Cloudina* found above the prominent negative value is proposed to be derived from previously deposited formations (Álvaro et al., 2019a). We tentatively suggest that the interval with the prominent negative value may correspond to the BACE, and acknowledge that a more detailed study with higher-resolution data would be needed to confirm this.

The Unit IV in the Ciudad Rodrigo-Hurdes-Sierra de Gata domain and the Ibor Group and Cíjara Formation in the Toledo-Alcudia Mountains are regionally correlated in Central Iberia (Valladares, 1995; Álvaro, 2020). The Unit IV, up to 500 m thick, is dominated by black shales, which has been suggested to represent deposition in a slope environment (Valladares, 1995). It contains a lenticular siliciclastic-carbonate level in its upper part, probably derived from the adjacent platform margin by turbidity currents (Valladares et al., 2006). The carbonate level in the Unit IV reveals similar $^{87}Sr/^{86}Sr$ ratios to the Villarta Formation (~0.7085; Valladares et al., 2006). The unconformably overlying Unit V is a calcareous megabreccia with blocks containing allochthonous *Cloudina* derived from previously deposited units (Valladares et al., 2006). Ichnofossils such as *Psammichnites* and small shelly fossils (aff. *Aldanella*) appear higher in the succession (Valladares et al., 2006). Therefore, Unit IV was proposed to be deposited close to the Ediacaran-Cambrian boundary (Valladares et al., 2006).

Valladares et al. (2006) reported a carbon isotope profile of the carbonate level in the Unit IV at Pastores (SW Salamanca, Central Iberia), which is about 25 m thick and mainly composed of bedded limestones and calcareous breccias. The $\delta^{13}C_{carb}$ values of the carbonate level range between −8.7‰ and −0.5‰ (Valladares et al., 2006), with a pronounced negative $\delta^{13}C_{carb}$ excursion in its lower part (Fig. 8). Although the concept of a BACE excursion had not yet been widely accepted (e.g. Zhu et al., 2006), they proposed that the negative excursion at Pastores could potentially be correlated with Ediacaran-Cambrian boundary sections in Mongolia, Oman and Morocco because of the overall comparable carbon and strontium isotope values. Nonetheless, Valladares et al. (2006) rejected the very negative $\delta^{13}C_{carb}$ values in the light of simultaneously increased Mn/Sr and $^{87}Sr/^{86}Sr$ ratios and negative covariation between $\delta^{13}C_{carb}$ and $^{87}Sr/^{86}Sr$ ratios from the same level. However, Mn/Sr may not always be a robust indicator for diagenetic alteration (Derry, 2010). The negative covariation between $\delta^{13}C_{carb}$ and $^{87}Sr/^{86}Sr$ ratios may also not necessarily suggest isotope resetting but could reflect a primary stratigraphic trend. Indeed a similar relationship has been observed during periods of negative $\delta^{13}C_{carb}$ values, such as the Shuram/DOUNCE (Sawaki et al., 2010) and WANCE excursions (B. Chen et al., 2022). Therefore, we consider that the $\delta^{13}C_{carb}$ values of the carbonate level are not significantly modified and retain those values for chemostratigraphic correlation. At Pastores, $\delta^{13}C_{carb}$ stabilizes at around −2‰ before plunging to −8.7‰. Similarly, $\delta^{13}C_{carb}$ of the Villarta Formation at Majada oscillates around −2‰ before a significant negative value of –8.4‰. Above the excursion, $\delta^{13}C_{carb}$ remains negative at both sections (Fig. 8). Combined with the discussion above, the similarity in $\delta^{13}C_{carb}$ profiles between Pastores and Majada thus supports correlation of the two stratigraphic units.

5.2.2. Global correlation

The Global Stratotype Section and Point (GSSP) of the Ediacaran-Cambrian boundary is located at the Fortune Head section, Burin Peninsula, Newfoundland, Canada at a level guided by the first appearance datum (FAD) of the complex trace fossil *Treptichnus pedum* (Brasier et al., 1994). However, the use of the FAD of *T. pedum* in the definition of the Cambrian base, in the absence of additional criteria, has been challenged due in large part to its strong facies dependence (e.g. Zhu et al., 2019; Peng et al., 2020; Topper et al., 2022; but see Buatois, 2018). Several other potential markers are thus proposed, including the FAD of typical Cambrian small shelly fossils, e.g. *Anabarites trisulcatus* and *Protoherzina anabarica*; the FAD of the *Asteridium-Heliosphaeridium-Comasphaeridium* (AHC) acritarch Assemblage; and the basal Cambrian carbon isotope excursion (BACE) (see Zhu et al., 2019 for a review). Nevertheless, the preservation of all of these fossils is also constrained by sedimentary facies and physiochemical conditions of sediments, and each of these comes with similar, or bigger problems, making the global correlation of biostratigraphy of the Ediacaran-Cambrian transition interval difficult. In this regard, the BACE excursion that has been found on multiple paleocontinents is becoming increasingly applied as an auxiliary means to recognize a horizon apparently close to the Ediacaran-Cambrian boundary as currently defined (e.g. Amthor et al., 2003; Bartley et al., 1998; Brasier et al., 1996; Hodgin et al., 2021; Maloof et al., 2005; Smith et al., 2016a; Topper et al., 2022; Zhu et al., 2003).

As shown in Fig. 9, the carbonate carbon isotope record at the Majada section can potentially be correlated with sections from Mongolia (Topper et al., 2022), USA (Smith et al., 2016a), South China (Li et al., 2013), Oman (Amthor et al., 2003) and Mexico (Hodgin et al.,

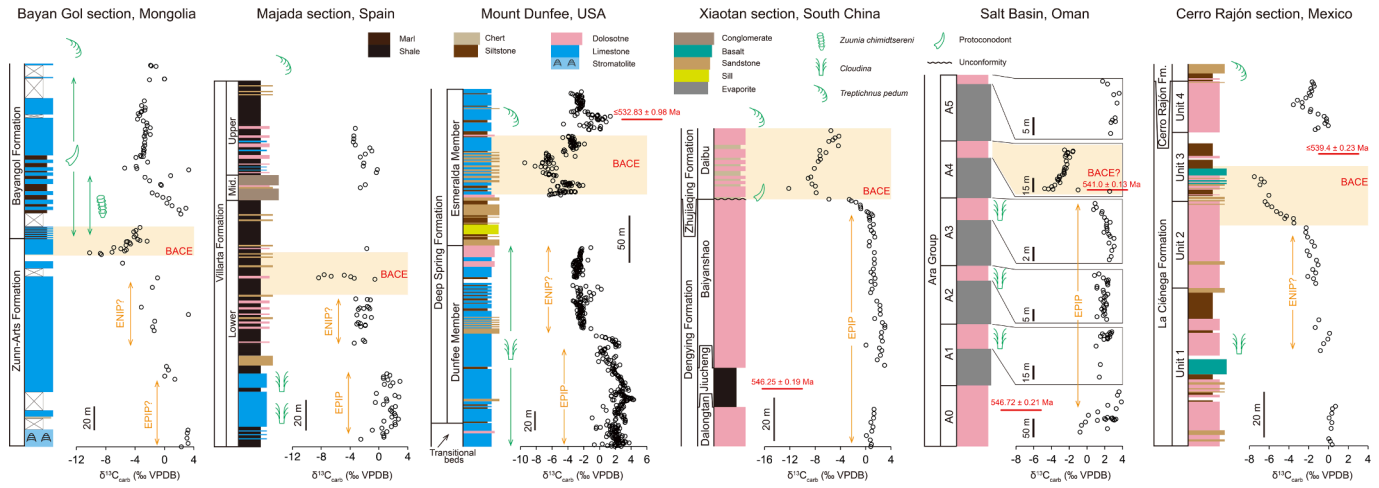

Fig. 9. Global carbonate carbon isotope stratigraphic correlation during the Ediacaran-Cambrian transition. The symbol of *T. pedum* above the stratigraphic columns indicates that they have been observed at a higher stratigraphic level. The Bayan Gol section is modified after Topper et al. (2022). The composite Mount Dunfee section is modified after Smith et al. (2016a), and the constraint of maximum depositional age for the recovery of BACE is from Nelson et al. (2023). At the Xiaotan section, the carbon isotope data are from Li et al. (2013), while the age constraint and occurrence of fossils are from Yang et al. (2021) and Yang et al. (2016), respectively. The carbon isotope data and age constraint for the Ara Group in the Salt Basin, Oman are from Amthor et al. (2003) and Bowring et al. (2007), respectively. The Cerro Rajón section is modified after Hodgin et al. (2021).

2021). All of these sections have independent evidence (e.g. fossil occurrences, radiometric dating, carbon and strontium isotope ratios) confirming that they straddle the Ediacaran-Cambrian boundary. The shape of $\delta^{13}C_{carb}$ profiles before the purported BACE excursion is similar for these sections in that there is a decreasing trend either abruptly or gradually from positive values to negative values (Fig. 9). The positive $\delta^{13}C_{carb}$ values oscillating around +2–4‰ before the BACE excursion are often referred to as the late Ediacaran positive carbon isotope plateau (EPIP; Zhu et al., 2017). Interestingly, new data from Mongolia, Spain, USA and Mexico reveal that the $\delta^{13}C_{carb}$ values decline to around −2‰ after the EPIP and remain relatively stable before the BACE excursion (Fig. 9), to which we tentatively refer as the late Ediacaran negative carbon isotope plateau (ENIP). The absence of the ENIP at Xiaotan (China) and in Oman can be attributed to depositional hiatuses before the BACE (Yang et al. 2016; Zhu et al., 2019), leading to incomplete $\delta^{13}C_{carb}$ profiles, although there is doubt whether the excursion in Oman truly represents the BACE (e.g. Hodgin et al., 2021; Bowyer et al., 2022; Nelson et al., 2022; Nelson et al., 2023). It thus appears to be evident that instead of plunging directly into the BACE from the EPIP, $\delta^{13}C_{carb}$ values exhibit a negative plateau before the excursion, which may be important for estimating the duration and magnitude of carbon isotope change. Although it is beyond the scope of this study, $\delta^{13}C_{carb}$ values lower than the average crustal carbon value would require additional isotopically light carbon input that may be derived from organic matter oxidation (e.g. Shields et al., 2019) and/or volcanism (Hodgin et al., 2021; Smith et al., 2023). Along with the presence of EPIP, ENIP, and BACE, it is clear that there were considerable perturbations to the global carbon cycle at this critical junction of biological evolution.

The ash bed near the zenith of the BACE excursion in the A4C member of the Ara Group in Oman yielded a zircon U–Pb CA–ID–TIMS age of 541.00 ± 0.13 Ma (Fig. 9; Bowring et al., 2007). More recently, the sandy dolostone bed that is 20 m above the nadir of the BACE excursion in the La Ciénega Formation, Mexico yielded a zircon U–Pb CA–ID–TIMS age of 539.40 ± 0.23 Ma, which is interpreted to represent the maximum depositional age (Fig. 9; Hodgin et al., 2021). By contrast, the Spitskop Member at Swartpunt in Namibia exhibits constant positive $\delta^{13}C_{carb}$ values at ~1‰, the ages of which have been constrained to be older than 538.58 ± 0.19 Ma by a zircon U–Pb CA–ID–TIMS age from an ash bed in the overlying Nomtsas Formation (Linnemann et al., 2019). To reconcile the age and carbon isotope discrepancies, Hodgin et al. (2021) proposed that the carbonate carbon isotope data from the Spitskop Member reflect a local, distinct dissolved inorganic carbon pool, whereas Nelson et al. (2022) suggested that the absence of the BACE in the upper Nama Group is because the excursion is younger than carbonates of the Schwarzrand Subgroup. In other words, they proposed that the BACE should be younger than 538 Ma based on high resolution carbonate carbon isotope data and zircon U–Pb CA–ID–TIMS ages of ash beds from the Schwarzrand Subgroup at the Neint Nababeep Plateau (South Africa). In Nevada, regional stratigraphic correlation and detrital zircon U–Pb CA–ID–TIMS ages from the lower Wood Canyon Formation also suggest the recovery of BACE younger than 532.83 ± 0.98 Ma (Nelson et al., 2023). It should however be noted that such young ages for the recovery of BACE place it close to the currently proposed ages of approximately 532–531 Ma for the base of Cambrian Stage 2 (e.g. Bowyer et al., 2022), seriously shortening the Fortunian Stage. Further to this, radiometric ages of approximately 532 Ma in New Brunswick overlie Cambrian-type trace fossils in the dated section and the most likely correlation of these New Brunswick ashes into Newfoundland is within the second Cambrian trace fossil zone (Hamilton et al., 2024). Assuming that *T. pedum* universally postdates BACE, this would either suggest that these young ages do not reflect the recovery of BACE or, invite the probably unlikely scenario of the recovery of BACE, the appearance of *T. pedum* and the base of Cambrian Stage 2 spanning a few million years or less.

5.3. *Nitrogen cycling across the Ediacaran-Cambrian transition in the Central Iberian Zone*

N_2 fixation by diazotrophs is the major source of nitrogen to the marine system. The nitrogen isotope fractionation associated with N_2 fixation is generally small ($\varepsilon_{product\text{-}reactant}$ = −2‰ to +1‰), leading to $\delta^{15}N$ of NH_4^+ close to that of atmospheric N_2 (~0‰; Stüeken et al., 2016), although alternative Fe- or V-nitrogenases can induce substantial isotope fractionation of −6‰ to −8‰ (Zhang et al., 2014). NH_4^+ undergoes microbially mediated oxidation to nitrite (ε = +14‰ to +38‰) and then nitrate (ε = −13‰) under oxic conditions (nitrification), with each step imparting significant isotope fractionation (Casciotti, 2009). However, such isotope fractionations are usually suppressed in modern oceans because nitrification is rapid and quantitative. The fixed nitrogen is converted into N_2/N_2O via denitrification ($NO_3^- \rightarrow N_2$) or anammox ($NO_2^- + NH_4^+ \rightarrow N_2$) occurring in suboxic water columns or pore waters with a significant isotope fractionation (ε > −25‰), which leaves the

residual NO_3^- pool isotopically heavier (Gruber and Sarmiento, 1997; Johnson et al., 2017). Under nitrate limited conditions, dissimilatory nitrate reduction to ammonium (DNRA; $NO_3^- \rightarrow NH_4^+$) is probably more favourable (Mettam and Zerkle, 2021), which also leads to residual NO_3^- enriched in ^{15}N (Chen et al., 2019). The balance of nitrogen input (N_2 fixation) and output (denitrification and anammox) ultimately controls the $\delta^{15}N$ values of marine biomass. In modern oceans, the $\delta^{15}N$ value is on average +5‰ (+3‰ to +14‰) signifying ~25 % or 32 % of NO_3^- denitrified to N_2 in the water column (Stüeken et al., 2016), whereas dynamic variations in ocean redox states and nutrient cycles through Earth's history can produce a wider range of $\delta^{15}N$ values in geological records (e.g. Wang et al., 2018).

The $\delta^{15}N$ values at Vía Verde mostly fluctuate at around +0.7‰ in the lower-middle part (possibly late Ediacaran) and show a decreasing trend from +0.98‰ to −1.49‰ in the upper part (possibly earliest Cambrian) of the Cíjara Formation (Fig. 3). The atmospheric-like $\delta^{15}N$ values (−2‰ to +1‰) are usually interpreted as (i) assimilation of NO_3^- in a fully oxygenated ocean with denitrification restricted in sediments and/or (ii) dominant N_2-fixation via Mo-based nitrogenase (e.g. Zerkle et al., 2008; Chen et al., 2019). The first scenario can be excluded here given that mounting evidence suggests dynamic redox variability of the atmospheric-ocean system during the Ediacaran-Cambrian transition interval (e.g. Zhang et al., 2018; Tostevin et al., 2019; Wei et al., 2020). Biological N_2-fixation converts N_2 into bioavailable NH_4^+, which can serve as the nutrient to be assimilated either partially or quantitatively (e.g. Higgins et al., 2012). However, as biomass favours incorporation of isotopically light N, partial assimilation of NH_4^+ can produce isotopically light biomass (<−2‰) and a heavy residual NH_4^+ pool (> +1‰) that can be sequestered in sediments elsewhere, which will lead to large isotopic fluctuations and spatial variability (Papineau et al., 2009; Chen et al., 2019; Wang et al., 2020). Such prediction is inconsistent with the observation in the Cíjara Formation whose $\delta^{15}N$ values are overall in the range of −2‰ to +1‰. Furthermore, abundant dissolved ammonium would suppress N_2 fixation because of its high energy demand (Stüeken et al., 2021), which would in turn prevent ammonium concentration from being too high, making quantitative assimilation of ammonium more likely. Therefore, the $\delta^{15}N$ in the Cíjara Formation at Vía Verde is most parsimoniously explained by dominant N_2-fixation with only modest recycling of an ammonium reservoir. When compared with the late Ediacaran-earliest Cambrian $\delta^{15}N$ values in South China (e.g. Wang et al., 2018), $\delta^{15}N$ data from the Cíjara Formation reveal a similar trend, i.e. relatively stable in the late Ediacaran and decreasing values through to the earliest Cambrian. However, the $\delta^{15}N$ values in the slope of South China are generally greater than +2.0‰ in the late Ediacaran (Chen et al., 2019), while contemporaneous Central Iberia shows $\delta^{15}N$ values generally lower than +1.0‰. This suggests a heterogeneous distribution of NO_3^- and/or NH_4^+ reservoirs in late Ediacaran oceans, and a shallower redox chemocline in Central Iberia. The negative shift of $\delta^{15}N$ in the earliest Cambrian could indicate expanded anoxia with further shoaling of the redox chemocline (e.g. Cremonese et al., 2013; Wang et al., 2018).

The $\delta^{15}N$ values are overall higher than +1.0‰ and can be as high as +4.6‰ in the lower part of the Pusa Formation (possible Fortunian Stage; Fig. 3), which is consistent with coeval $\delta^{15}N$ data from South China (e.g. Wang et al., 2018; Wei et al., 2021). The high positive $\delta^{15}N$ values are often attributed to (i) partial nitrification followed by quantitative assimilation of NH_4^+ and NO_3^-, (ii) partial assimilation of NO_3^- and/or NH_4^+, and (iii) partial removal of fixed nitrogen, i.e. denitrification, anammox, or DNRA (e.g. Ader et al., 2016; Stüeken et al., 2016; Chen et al., 2019). While partial nitrification has only been reported in the modern Bering Sea with seasonally variable oxygen contents (Granger et al., 2011; Morales et al., 2014), partial assimilation mostly occurs today at high latitudes and equatorial upwelling zones with abundant NO_3^- (Tesdal et al., 2013). Furthermore, the first and second scenarios would require the existence of both ^{15}N depleted (negative) and enriched (positive) records (e.g. Chen et al., 2019), which has not been observed so far in the Pusa Formation. In a redox stratified water column that is typical of the Ediacaran-Cambrian ocean (e.g. Shields, 2017), partial removal of fixed nitrogen occurs at the oxic/suboxic interface, rendering the residual NO_3^- pool in shallow seawater enriched in ^{15}N (Kritee et al., 2012; Stüeken et al., 2021). Once utilized by nitrate assimilators, the high positive $\delta^{15}N$ values can be transferred into sediments. However, such a signal can only be expressed when there is a stable nitrate reservoir; otherwise N_2 fixation triggered by N limitation due to intense N loss would dominate $\delta^{15}N$ signals (e.g. Kipp et al., 2018). Therefore, the $\delta^{15}N$ data fluctuating at ~1.5‰ with punctuated high positive values in the Pusa Formation are mostly consistent with a temporally varied small to moderate nitrate reservoir and aerobic N cycling during its deposition. Overall, the $\delta^{15}N$ data suggest that the nitrogen biogeochemical cycle in Central Iberia likely transformed from predominantly anaerobic to aerobic recycling during deposition of the Cíjara through Pusa formations, although we stress that more analyses at higher resolution and from different local sections are needed to delineate the full picture of N cycling in Central Iberia.

5.4. Implications for biotic turnover across the Ediacaran-Cambrian transition

Ediacaran biota represents the first radiation of large, complex multicellular eukaryotes including animal groups seemingly without modern representatives. They disappeared across the Ediacaran-Cambrian transition to be succeeded by successive radiations of Cambrian biota (the 'Cambrian Explosion'), representing the appearance of many extant animal clades (e.g. Xiao and Laflamme, 2009). Either pulsed extinction due to dramatic environmental changes or gradual biotic replacement due to resource competition and ecosystem engineering has been proposed to give rise to this biotic turnover, although these two may not be mutually exclusive (e.g. Amthor et al., 2003; Laflamme et al., 2013; Darroch et al., 2015; Darroch et al., 2023; Mussini and Dunn, 2023).

The terminal Ediacaran biota is characterized by a reduction in soft-bodied macrofossil diversity as well as the appearance of organic-walled and skeletal tubular fossils (Jensen et al., 2006). Recent progress reveals the temporal overlap between some typical late Ediacaran skeletal fossils and small skeletal fossils commonly interpreted as Cambrian in age (e.g. Bowyer et al., 2023). In Mongolia, the cloudinid *Zuunia chimidtsereni* co-occurs with the protoconodont *Protohertzina anabarica* in the lower Bayangol Formation above the BACE excursion (Fig. 9; Topper et al., 2022). In South China, *Cloudina* was found to co-occur with *Anabarites trisulcatus* in the lower Kuanchuanpu Formation (Yang et al., 2016), but their exact position relative to the BACE remains uncertain (Bowyer et al., 2022). The terminal Ediacaran Dengying Formation at Lijiagou in South China also records the co-occurrence of *Cloudina* and *Sinotubulites* with possible early Cambrian shelly fossils, similar to *Anabarites trisulcatus* (Cai et al., 2019). In Siberia, typical Ediacaran and Cambrian skeletal fossils (*Cloudina, Anabarites, Protohertzina*) have been recovered from the Ust'-Yudoma Formation at Kyra-Ytyga, which is thought to have been deposited before the BACE excursion (Zhu et al., 2017), although the assignment of an Ediacaran age for the formation has recently been questioned (Topper et al., 2022). Bowyer et al. (2023) elaborated two age models for the Kyra-Ytyga cloudinids in which they are either pre-BACE or late Fortunian. They do not express a preference for either model but note that a late Fortunian age would be exceptionally young for the genus. In line with earlier studies they stress the co-occurrence of what has been traditionally viewed as distinct Ediacaran and Cambrian faunal elements at the Kyra-Ytyga section. In the Nama Group of Namibia and South Africa, the BACE excursion has not been identified, possibly because the Schwarzrand carbonates are older than the excursion (Nelson et al., 2022). The proposed Ediacaran-Cambrian boundary there is defined by the occurrence of complex trace fossils with an age of ca. 538.8 Ma (Linnemann et al., 2019; Peng et al., 2020), although a higher placement of the boundary can also be argued for. Some relatively complex trace fossils have also been found

below the proposed boundary, while the stratigraphically highest occurrences of *Cloudina* postdate the first *Treptichnus* in the Urusis Formation, with undoubted *Treptichnus pedum* first appearing in the overlying Nomtsas Formation (e.g. Jensen et al., 2000; Jensen and Runnergar, 2005; Buatois et al., 2018; Nelson et al., 2022). The morphologically complex trace fossil *Streptichnus* dated at about 539 Ma overlaps the range of *Cloudina* (Linnemann et al. 2019). Overall, these paleontological findings thus suggest a stronger evolutionary connection than previously thought between typical Ediacaran and Cambrian biotas.

Nonetheless, we highlight that although the tubular skeletal fossils, e.g. *Zuunia chimidtsereni*, can occur above the BACE excursion, the typical late Ediacaran index fossil, *Cloudina*, has not been found above the BACE excursion (unless this is the case at Kyra-Ytaga), while cloudinids have also not been found unambiguously to co-occur with *Treptichnus pedum*. Furthermore, it appears that *T. pedum* is exclusively found above the BACE excursion in successions where both the BACE and *T. pedum* have been anchored (Fig. 9), possibly reflecting a genuine evolutionary order of these key marker fossils. Regardless of the two possible positions for the BACE excursion in Central Iberia (Fig. 8), the occurrence of *Treptichnus pedum* and autochthonous *Cloudina* is found stratigraphically above and below the BACE, respectively (Fig. 8), reinforcing the emerging temporal framework of index fossils during the Ediacaran-Cambrian transition interval.

6. Conclusions

We present geochemical data from two carbonate-siliciclastic sections straddling the Ediacaran-Cambrian interval in Central Iberia, Spain. Given the biostratigraphic context and the fidelity of measured carbon isotope trends, the negative carbon isotope excursion in the lower member of the Villarta Formation at Majada possibly represents the basal Cambrian carbon isotope excursion (BACE). The lower Villarta Formation at Majada also reveals a rise from negative to low positive $\delta^{13}C_{carb}$ values, which is associated with the first appearance of *Cloudina* and the most pristine $^{87}Sr/^{86}Sr$ ratio of 0.708512, indicating that the lower Villarta Formation is correlative with the terminal Ediacaran strata in China and Namibia. $\delta^{15}N$ data from the Vía Verde section reveal a similar trend to that reported from South China during the Ediacaran-Cambrian transition interval, but show relatively lower values in the late Ediacaran. We suggest that nitrogen cycling in Central Iberia possibly evolved from anaerobic to aerobic across the Ediacaran-Cambrian transition, although this needs to be constrained by more analyses from correlative successions.

Based on the global correlation of sections across the Ediacaran-Cambrian transition interval, it seems that the first appearance of *Treptichnus pedum* exclusively occurs stratigraphically above the BACE excursion, while the last appearance of the late Ediacaran index fossil *Cloudina* has so far only been found below the BACE excursion. The emerging global chemostratigraphic framework also indicates a negative $\delta^{13}C$ plateau before the BACE excursion. The presence of late Ediacaran positive and negative plateaus and the BACE excursion suggest that the global carbon cycle experienced significant perturbations across the Ediacaran-Cambrian transition interval.

CRediT authorship contribution statement

Kun Zhang: Writing – review & editing, Writing – original draft, Visualization. **Graham A. Shields:** Writing – review & editing, Supervision, Resources, Investigation, Funding acquisition. **Ying Zhou:** Writing – review & editing, Investigation. **Harald Strauss:** Resources, Investigation. **Ulrich Struck:** Resources, Investigation, Funding acquisition. **Sören Jensen:** Writing – review & editing, Investigation, Funding acquisition.

Declaration of competing interest

The authors declare that they have no known competing financial interests or personal relationships that could have appeared to influence the work reported in this paper.

Data availability

Data are available in the supplementary material.

Acknowledgments

This work was funded by the Spanish Ministry of Science and Innovation (MICINN) through grants CGL2004-02967 and CGL2008-04374 (cofinanced by Fondo Europeo de Desarollo Regional [FEDER]). SJ acknowledges current funding from PID2021-125585NB-I00 of the Spanish Ministry of Science and Innovation. GS and US acknowledge funding from the German Research Foundation (DFG) as part of a Sino-German Research Project FOR 736. GS additionally acknowledges funding from the NERC BETR programme (NE/PO13643/1) in support of this study. We are grateful to the owners of the Majada de Andaluz for allowing us access to their property. We thank two anonymous reviewers for constructive suggestions that improved this manuscript, and Frances Westall for editorial assistance.

Appendix A. Supplementary data

Supplementary data to this article can be found online at https://doi.org/10.1016/j.precamres.2024.107526.

References

Ader, M., Thomazo, C., Sansjofre, P., Busigny, V., Papineau, D., Laffont, R., Cartigny, P., Halverson, G.P., 2016. Interpretation of the nitrogen isotopic composition of Precambrian sedimentary rocks: Assumptions and perspectives. Chem. Geol. 429, 93–110.

Álvaro, J.J., 2020. Calibrating $\delta^{13}C$ and $\delta^{18}O$ chemostratigraphic correlations across Cambrian strata of SW Europe and Morocco, West Gondwana. In: Stratigraphy & Timescales. Elsevier Inc., pp. 269–317

Álvaro, J.J., Shields-Zhou, G.A., Ahlberg, P., Jensen, S., Palacios, T., 2016. Ediacaran-Cambrian phosphorites from the western margins of gondwana and baltica. Sedimentology 63, 350–377.

Álvaro, J.J., Cortijo, I., Jensen, S., Lorenzo, S., Pieren, A.P., 2019a. Updated stratigraphic framework and biota of the Ediacaran and Terreneuvian in the Alcudia-Toledo Mountains of the Central Iberian Zone, Spain. *Estudios Geológicos* 75, 093.

Álvaro, J.J., Jensen, S., Palacios, T., 2019b. Post-conference fieldtrip, October 21–24, 2019: Ediacaran and Terreneuvian strata surrounding the Villuercas-Ibores-Jara UNESCO global geopark. Estudios Geológicos 75, 121.

Álvaro, J.J., Cortijo, I., Jensen, S., Martí Mus, M., Palacios, T., 2020. *Cloudina*-microbial reef resilience to substrate instability in a Cadomian retro-arc basin of the Iberian Peninsula. Precambrian Res. 336, 105479.

Álvaro, J.J., Jensen, S., Valverde-Vaquero, P., 2024. Multidisciplinary re-assessment of the Ediacaran-Cambrian boundary interval in south-western Europe. Newsl Stratigr. 57, 323–357.

Amthor, J.E., Grotzinger, J.P., Schröder, S., Bowring, S.A., Ramezani, J., Martin, M.W., Matter, A., 2003. Extinction of *Cloudina* and *Namacalathus* at the Precambrian-Cambrian boundary in Oman. Geology 31, 431–434.

Banner, J.L., Hanson, G.N., 1990. Calculation of simultaneous isotopic and trace element variations during water-rock interaction with applications to carbonate diagenesis. Geochim. Cosmochim. Acta 54, 3123–3137.

Bartley, J.K., Pope, M., Knoll, A.H., Semikhatov, M.A., Petrov, P.Y., 1998. A Vendian-Cambrian boundary succession from the northwestern margin of the Siberian Platform: Stratigraphy, palaeontology, chemostratigraphy and correlation. Geol. Mag. 135, 473–494.

Bold, U., Ahm, A.S.C., Schrag, D.P., Higgins, J.A., Jamsran, E., Macdonald, F.A., 2020. Effect of dolomitization on isotopic records from Neoproterozoic carbonates in southwestern Mongolia. Precambrian Res. 350, 105902.

Bowring, S.A., Grotzinger, J.P., Condon, D.J., Ramezani, J., Newall, M.J., Allen, P.A., 2007. Geochronologic constraints on the chronostratigraphic framework of the Neoproterozoic Huqf Supergroup, Sultanate of Oman. Am. J. Sci. 307, 1097–1145.

Bowyer, F.T., Zhuravlev, A.Y., Wood, R., Shields, G.A., Zhou, Y., Curtis, A., Poulton, S. W., Condon, D.J., Yang, C., Zhu, M., 2022. Calibrating the temporal and spatial dynamics of the Ediacaran - Cambrian radiation of animals. Earth-Science Rev. 225, 103913.

Bowyer, F.T., Zhuravlev, A.Y., Wood, R., Zhao, F., Sukhov, S.S., Alexander, R.D., Poulton, S.W., Zhu, M., 2023. Implications of an integrated late Ediacaran to early Cambrian stratigraphy of the Siberian Platform Russia. GSA Bull. 2428–2450.
Brand, U., Veizer, J., 1980. Chemical diagenesis of a multicomponent carbonate system–1: Trace elements. J. Sediment. Res. 50, 987–998.
Brasier, M., Cowie, J., Taylor, M., 1994. Decision on the Precambrian-Cambrian boundary stratotype. Episodes 17, 3–8.
Brasier, M.D, Perejón, A., de San José, M.A., 1979. Discovery of an important fossiliferous Precambrian–Cambrian sequence in Spain. Estudios Geológicos 35, 379–383.
Brasier, M.D., Shields, G., Kuleshov, V.N., Zhegallo, E.A., 1996. Integrated chemo- and biostratigraphic calibration of early animal evolution: Neoproterozoic–early Cambrian of southwest Mongolia. Geol. Mag. 133, 445–485.
Buatois, L.A., 2018. *Treptichnus pedum* and the Ediacaran-Cambrian boundary: Significance and caveats. Geol. Mag. 155, 174–180.
Buatois, L.A., Almond, J., Mángano, M.G., Jensen, S., Germs, G.J.B., 2018. Sediment disturbance by Ediacaran bulldozers and the roots of the Cambrian explosion. Sci. Rep. 8, 1–9.
Cai, Y., Xiao, S., Li, G., Hua, H., 2019. Diverse biomineralizing animals in the terminal Ediacaran Period herald the Cambrian explosion. Geology 47, 380–384.
Casciotti, K.L., 2009. Inverse kinetic isotope fractionation during bacterial nitrite oxidation. Geochim. Cosmochim. Acta 73, 2061–2076.
Chen, Y., Diamond, C.W., Stüeken, E.E., Cai, C., Gill, B.C., Zhang, F., Bates, S.M., Chu, X., Ding, Y., Lyons, T.W., 2019. Coupled evolution of nitrogen cycling and redoxcline dynamics on the Yangtze Block across the Ediacaran-Cambrian transition. Geochim. Cosmochim. Acta 257, 243–265.
Chen, B., Hu, C., Mills, B.J.W., He, T., Andersen, M.B., Chen, X., Liu, P., Lu, M., Newton, R.J., Poulton, S.W., Shields, G.A., Zhu, M., 2022. A short-lived oxidation event during the early Ediacaran and delayed oxygenation of the Proterozoic ocean. Earth Planet. Sci. Lett. 577, 117274.
Chen, X., Zhou, Y., Shields, G.A., 2022. Progress towards an improved Precambrian seawater $^{87}Sr/^{86}Sr$ curve. Earth-Science Rev. 224, 103869.
Cortijo, I., Martí Mus, M., Jensen, S., Palacios, T., 2010. A new species of *Cloudina* from the terminal Ediacaran of Spain. Precambrian Res. 176, 1–10.
Cortijo, I., Martí Mus, M., Jensen, S., Palacios, T., 2015. Late Ediacaran skeletal body fossil assemblage from the Navalpino anticline, central Spain. Precambrian Res. 267, 186–195.
Cremonese, L., Shields-Zhou, G., Struck, U., Ling, H.F., Och, L., Chen, X., Li, D., 2013. Marine biogeochemical cycling during the early Cambrian constrained by a nitrogen and organic carbon isotope study of the Xiaotan section. South China. *Precambrian Res.* 225, 148–165.
Darroch, S.A.F., Sperling, E.A., Boag, T.H., Racicot, R.A., Mason, S.J., Morgan, A.S., Tweedt, S., Myrow, P., Johnston, D.T., Erwin, D.H., Laflamme, M., 2015. Biotic replacement and mass extinction of the Ediacara biota. Proc. r. Soc. B Biol. Sci. 282, 20151003.
Darroch, S.A.F., Smith, E.F., Laflamme, M., Erwin, D.H., 2018. Ediacaran extinction and Cambrian explosion. Trends Ecol. Evol. 33, 653–663.
Darroch, S.A.F., Smith, E.F., Nelson, L.L., Craffey, M., Schiffbauer, J.D., Laflamme, M., 2023. Causes and consequences of end-Ediacaran extinction – an update. Cambridge Prism. Extinction 1, 1–15.
Derry, L.A., 2010. A burial diagenesis origin for the Ediacaran Shuram-Wonoka carbon isotope anomaly. Earth Planet. Sci. Lett. 294, 152–162.
Erwin, D.H., Laflamme, M., Tweedt, S.M., Sperling, E.A., Pisani, D., Peterson, K.J., 2011. The Cambrian conundrum: Early divergence and later ecological success in the early history of animals. Science 334, 1091–1097.
Freudenthal, T., Wagner, T., Wenzhöfer, F., Zabel, M., Wefer, G., 2001. Early diagenesis of organic matter from sediments of the Eastern subtropical Atlantic: Evidence from stable nitrogen and carbon isotopes. Geochim. Cosmochim. Acta 65, 1795–1808.
Granger, J., Prokopenko, M.G., Sigman, D.M., Mordy, C.W., Morse, Z.M., Morales, L.V., Sambrotto, R.N., Plessen, B., 2011. Coupled nitrification-denitrification in sediment of the eastern Bering Sea shelf leads to ^{15}N enrichment of fixed N in shelf waters. J. Geophys. Res. Ocean. 116, 1–18.
Gruber, N., Sarmiento, J.L., 1997. Global patterns of marine nitrogen fixation and denitrification. Global Biogeochem. Cycles 11, 235–266.
Hamilton, M.A., Álvaro, J.J., Barr, S.M., Jensen, S., Johnson, S.C., Palacios, T., van Rooyen, D., White, C.E., 2024. U-Pb zircon ages from tuffaceous beds in the Terreneuvian to Cambrian Series 2 sections of Avalonian southern New Brunswick, Canada: new constraints on chronostratigraphic correlations and the Cambrian time scale. Geol. Soc. London, Spec. Publ. 542, 217–232.
Higgins, M.B., Robinson, R.S., Husson, J.M., Carter, S.J., Pearson, A., 2012. Dominant eukaryotic export production during ocean anoxic events reflects the importance of recycled NH^{4+}. Proc. Natl. Acad. Sci. U. S. A. 109, 2269–2274.
Hodgin, E.B., Nelson, L.L., Wall, C.J., Barrón-Díaz, A.J., Webb, L.C., Schmitz, M.D., Fike, D.A., Hagadorn, J.W., Smith, E.F., 2021. A link between rift-related volcanism and end-Ediacaran extinction? Integrated chemostratigraphy, biostratigraphy, and U-Pb geochronology from Sonora, Mexico. Geology 49, 115–119.
Hood, A.v.S., Planavsky, N.J., Wallace, M.W., Wang, X., 2018. The effects of diagenesis on geochemical paleoredox proxies in sedimentary carbonates. Geochim. Cosmochim. Acta 232, 265–287.
Horita, J., 2014. Oxygen and carbon isotope fractionation in the system dolomite-water-CO_2 to elevated temperatures. Geochim. Cosmochim. Acta 129, 111–124.
Jensen, S., Palacios, T., 2016. The Ediacaran-Cambrian trace fossil record in the Central Iberian Zone, Iberian Peninsula O registo icnológico do Ediacariano-Câmbrico da Zona Centro- Ibérica, Península Ibérica. *Comun. Geológicas* 103, 83–92.
Jensen, S., Palacios, T., Martí Mus, M., 2007. A brief review of the fossil record of the ediacaran-cambrian transition in the area of montes de toledo-guadalupe, spain. *Geol. Soc. Spec. Publ.* 286, 223–235.
Jensen, S., Palacios, T., Mus, M.M., 2010. Revised biochronology of the Lower Cambrian of the Central Iberian zone, southern Iberian massif, Spain. *Geol. Mag.* 147, 690–703.
Jensen, S., Runnergar, B.N., 2005. A complex trace fossil from the spitskop member (terminal Ediacaran-? Lower Cambrian) of southern Namibia. Geol. Mag. 142, 561–569.
Jensen, S., Saylor, B.Z., Gehling, J.G., Germs, G.J.B., 2000. Complex trace fossils from terminal Proterozoic of Namibia. Geology 28, 143–146.
Jensen, S., Droser, M.L., Gehling, J.G., 2006. A critical look at the ediacaran trace fossil record. Neoproterozoic Geobiol. Paleobiol. 115–157.
Johnson, B.W., Poulton, S.W., Goldblatt, C., 2017. Marine oxygen production and open water supported an active nitrogen cycle during the Marinoan Snowball Earth. Nat. Commun. 8, 1–10.
Kaufman, A.J., Knoll, A.H., 1995. Neoproterozoic variations in the C-isotopic composition of seawater: stratigraphic and biogeochemical implications. Precambrian Res. 73, 27–49.
Kipp, M.A., Stüeken, E.E., Yun, M., Bekker, A., Buick, R., 2018. Pervasive aerobic nitrogen cycling in the surface ocean across the Paleoproterozoic Era. Earth Planet. Sci. Lett. 500, 117–126.
Kritee, K., Sigman, D.M., Granger, J., Ward, B.B., Jayakumar, A., Deutsch, C., 2012. Reduced isotope fractionation by denitrification under conditions relevant to the ocean. Geochim. Cosmochim. Acta 92, 243–259.
Kuznetsov, A.B., Bekker, A., Ovchinnikova, G.V., Gorokhov, I.M., Vasilyeva, I.M., 2017. Unradiogenic strontium and moderate-amplitude carbon isotope variations in early Tonian seawater after the assembly of Rodinia and before the Bitter springs excursion. Precambrian Res. 298, 157–173.
Laflamme, M., Darroch, S.A.F., Tweedt, S.M., Peterson, K.J., Erwin, D.H., 2013. The end of the Ediacara biota: Extinction, biotic replacement, or Cheshire Cat? Gondwana Res. 23, 558–573.
Lau, K.V., Hardisty, D.S., 2022. Modeling the impacts of diagenesis on carbonate paleoredox proxies. Geochim. Cosmochim. Acta 337, 123–139.
Li, D., Ling, H.F., Shields-Zhou, G.A., Chen, X., Cremonese, L., Och, L., Thirlwall, M., Manning, C.J., 2013. Carbon and strontium isotope evolution of seawater across the Ediacaran-Cambrian transition: Evidence from the Xiaotan section, NE yunnan South China. Precambrian Res. 225, 128–147.
Liñán, E., Gámez Vintaned, J.A., Palacios, T., Gozalo, R., 2020. The lower Ovetian Stage (lower Cambrian Stage 3) trilobite zonation in Spain and correlation with West Gondwana. GFF 142, 100–114.
Linnemann, U., Pidal, A.P., Hofmann, M., Drost, K., Quesada, C., Gerdes, A., Marko, L., Gärtner, A., Zieger, J., Ulrich, J., Krause, R., Vickers-Rich, P., Horak, J., 2018. A ~565 Ma old glaciation in the Ediacaran of peri-Gondwanan West Africa. Int. J. Earth Sci. 107, 885–911.
Linnemann, U., Ovtcharova, M., Schaltegger, U., Gärtner, A., Hautmann, M., Geyer, G., Vickers-Rich, P., Rich, T., Plessen, B., Hofmann, M., Zieger, J., Krause, R., Kriesfeld, L., Smith, J., 2019. New high-resolution age data from the Ediacaran-Cambrian boundary indicate rapid, ecologically driven onset of the Cambrian explosion. Terra Nov. 31, 49–58.
Maloof, A.C., Schrag, D.P., Crowley, J.L., Bowring, S.A., 2005. An expanded record of Early Cambrian carbon cycling from the Anti-Atlas Margin, Morocco. Can. J. Earth Sci. 42, 2195–2216.
McArthur, J.M., Howarth, R.J., Shields, G.A., Zhou, Y., 2020. Strontium Isotope Stratigraphy, in: Geologic Time Scale 2020. Elsevier, pp. 211–238.
McCrea, J.M., 1950. On the isotopic chemistry of carbonates and a paleotemperature scale. J. Chem. Phys. 18, 849–857.
Mettam, C., Zerkle, A.L., 2021. Nitrogen Isotopes in Deep Time. Cambridge University Press.
Mettam, C., Zerkle, A.L., Claire, M.W., Prave, A.R., Poulton, S.W., Junium, C.K., 2019. Anaerobic nitrogen cycling on a Neoarchaean ocean margin. Earth Planet. Sci. Lett. 527, 115800.
Morales, L.V., Granger, J., Chang, B.X., Prokopenko, M.G., Plessen, B., Gradinger, R., Sigman, D.M., 2014. Elevated $^{15}N/^{14}N$ in particulate organic matter, zooplankton, and diatom frustule-bound nitrogen in the ice-covered water column of the Bering Sea eastern shelf. Deep Sea Res Part II Top. Stud. Oceanogr 109, 100–111.
Mussini, G., Dunn, F.S., 2023. Decline and fall of the Ediacarans: late-Neoproterozoic extinctions and the rise of the modern biosphere. Biol. Rev. 1, 110–130.
Nelson, L.L., Ahm, A.S.C., Macdonald, F.A., Higgins, J.A., Smith, E.F., 2021. Fingerprinting local controls on the Neoproterozoic carbon cycle with the isotopic record of Cryogenian carbonates in the Panamint Range, California. Earth Planet. Sci. Lett. 566.
Nelson, L.L., Ramezani, J., Almond, J.E., Darroch, S.A.F., Taylor, W.L., Brenner, D.C., Furey, R.P., Turner, M., Smith, E.F., 2022. Pushing the boundary: A calibrated Ediacaran-Cambrian stratigraphic record from the Nama Group in northwestern Republic of South Africa. Earth Planet. Sci. Lett. 580, 117396.
Nelson, L.L., Crowley, J.L., Smith, E.F., Schwartz, D.M., Hodgin, E.B., Schmitz, M.D., 2023. Cambrian explosion condensed: High-precision geochronology of the lower Wood Canyon Formation, Nevada. Proc. Natl. Acad. Sci. 120, 2017.
Ossa Ossa, F., Hofmann, A., Wille, M., Spangenberg, J.E., Bekker, A., Poulton, S.W., Eickmann, B., Schoenberg, R., 2018. Aerobic iron and manganese cycling in a redox-stratified Mesoarchean epicontinental sea. Earth Planet. Sci. Lett. 500, 28–40.
Papineau, D., Purohit, R., Goldberg, T., Pi, D., Shields, G.A., Bhu, H., Steele, A., Fogel, M. L., 2009. High primary productivity and nitrogen cycling after the Paleoproterozoic phosphogenic event in the Aravalli Supergroup. India. *Precambrian Res.* 171, 37–56.
Peng, S.C., Babcock, L.E., Ahlberg, P., 2020. The Cambrian Period, in: Geologic Time Scale 2020. Elsevier, pp. 565–629.

Sawaki, Y., Ohno, T., Tahata, M., Komiya, T., Hirata, T., Maruyama, S., Windley, B.F., Han, J., Shu, D., Li, Y., 2010. The Ediacaran radiogenic Sr isotope excursion in the Doushantuo Formation in the Three Gorges area. South China. *Precambrian Res.* 176, 46–64.
Scotese, C.R., 2021. An atlas of Phanerozoic paleogeographic maps: The seas come in and the seas go out. Annu. Rev. Earth Planet. Sci. 49, 679–728.
Shields, G.A., 2017. Earth system transition during the Tonian-Cambrian interval of biological innovation: Nutrients, climate, oxygen and the marine organic carbon capacitor. Geol. Soc. Spec. Publ. 448, 161–177.
Shields, G.A., Mills, B.J.W., Zhu, M., Raub, T.D., Daines, S.J., Lenton, T.M., 2019. Unique Neoproterozoic carbon isotope excursions sustained by coupled evaporite dissolution and pyrite burial. Nat. Geosci. 12, 823–827.
Shields, G., Stille, P., Brasier, M.D., Atudorei, N., 1997. Stratified oceans and oxygenation of the late Precambrian environment: a post glacial geochemical record from the Neoproterozoic of W. Mongolia. *Terra Nov.* 9, 218–222.
Smith, E.F., Nelson, L.L., Strange, M.A., Eyster, A.E., Rowland, S.M., Schrag, D.P., Macdonald, F.A., 2016a. The end of the Ediacaran: Two new exceptionally preserved body fossil assemblages from Mount Dunfee, Nevada, USA. Geology 44, 911–914.
Smith, E.F., Macdonald, F.A., Petach, T.A., Bold, U., Schrag, D.P., 2016b. Integrated stratigraphic, geochemical, and paleontological late Ediacaran to early Cambrian records from southwestern Mongolia. Geol. Soc. Am. Bull. 128, 442–468.
Smith, E.F., Nelson, L.L., O'Connell, N., Eyster, A., Lonsdale, M.C., 2023. The Ediacaran–Cambrian transition in the southern Great Basin. United States. *GSA Bull.* 135, 1393–1414.
Stüeken, E.E., Kipp, M.A., Koehler, M.C., Buick, R., 2016. The evolution of Earth's biogeochemical nitrogen cycle. Earth-Science Rev. 160, 220–239.
Stüeken, E.E., Kuznetsov, A.B., Vasilyeva, I.M., Krupenin, M.T., Bekker, A., 2021. Transient deep-water oxygenation recorded by rare Mesoproterozoic phosphorites. South Urals. *Precambrian Res.* 360, 106242.
Swart, P.K., 2015. The geochemistry of carbonate diagenesis: The past, present and future. Sedimentology 62, 1233–1304.
Talavera, C., Montero, P., Martínez Poyatos, D., Williams, I.S., 2012. Ediacaran to Lower Ordovician age for rocks ascribed to the Schist-Graywacke Complex (Iberian Massif, Spain): Evidence from detrital zircon SHRIMP U-Pb geochronology. Gondwana Res. 22, 928–942.
Talavera, C., Martínez Poyatos, D., González Lodeiro, F., 2015. SHRIMP U-Pb geochronological constraints on the timing of the intra-Alcudian (Cadomian) angular unconformity in the Central Iberian Zone (Iberian Massif, Spain). Int. J. Earth Sci. 104, 1739–1757.
Tesdal, J.E., Galbraith, E.D., Kienast, M., 2013. Nitrogen isotopes in bulk marine sediment: Linking seafloor observations with subseafloor records. Biogeosciences 10, 101–118.
Topper, T., Betts, M.J., Dorjnamjaa, D., Li, G., Li, L., Altanshagai, G., Enkhbaatar, B., Skovsted, C.B., 2022. Locating the BACE of the Cambrian: Bayan Gol in southwestern Mongolia and global correlation of the Ediacaran-Cambrian boundary. Earth-Science Rev. 229, 104017.
Torsvik, T.H., Rehnström, E.F., 2001. Cambrian palaeomagnetic data from Baltica: Implications for true polar wander and Cambrian palaeogeography. J. Geol. Soc. London. 158, 321–330.
Tostevin, R., Clarkson, M.O., Gangl, S., Shields, G.A., Wood, R.A., Bowyer, F., Penny, A. M., Stirling, C.H., 2019. Uranium isotope evidence for an expansion of anoxia in terminal Ediacaran oceans. Earth Planet. Sci. Lett. 506, 104–112.
Tucker, M.E., 1986. Formerly aragonitic limestones associated with tillites in the late Proterozoic of Death Valley. California. J. Sediment. Res. 56, 818–830.
Vahrenkamp, V.C., Swart, P.K., 1990. New distribution coefficient for the incorporation of strontium into dolomite and its implications for the formation of ancient dolomites. Geology 18, 387–391.
Valladares, M.I., 1995. Siliciclastic-carbonate slope apron in an immature tensional margin (Upper Precambrian-Lower Cambrian), Central Iberian Zone, Salamanca, Spain. Sediment. Geol. 94, 165–186.
Valladares, M.I., Ugidos, J.M., Barba, P., Fallick, A.E., Ellam, R.M., 2006. Oxygen, carbon and strontium isotope records of Ediacaran carbonates in Central Iberia (Spain). Precambrian Res. 147, 354–365.
Vidal, G., Jensen, S., Palacios, T., 1994a. Neoproterozoic (Vendian) ichnofossils from Lower Alcudian strata in central Spain. Geol. Mag. 131, 169–179.
Vidal, G., Palacios, T., Gámez-Vintaned, J.A., Balda, M.A.D., Grant, S.W.F., 1994b. Neoproterozoic-early Cambrian geology and palaeontology of Iberia. Geol. Mag. 131, 729–765.
Wachter, E.A., Hayes, J.M., 1985. Exchange of oxygen isotopes in carbon dioxide-phosporic acid systems. Chem. Geol. Isot. Geosci. Sect. 52, 365–374.
Wang, D., Ling, H.-F., Struck, U., Zhu, X.-K., Zhu, M., He, T., Yang, B., Gamper, A., Shields, G.A., 2018. Coupling of ocean redox and animal evolution during the Ediacaran-Cambrian transition. Nat. Commun. 9, 2575.
Wang, Z., Wang, X., Shi, X., Tang, D., Stüeken, E.E., Song, H., 2020. Coupled nitrate and phosphate availability facilitated the expansion of eukaryotic life at circa 1.56 Ga. J. Geophys. Res Biogeosciences 125.
Wei, G., Planavsky, N.J., Tarhan, L.G., He, T., Wang, D., Shields, G.A., Wei, W., Ling, H.-F., 2020. Highly dynamic marine redox state through the Cambrian explosion highlighted by authigenic $\delta^{238}U$ records. Earth Planet. Sci. Lett. 544, 116361.
Wei, G.Y., Planavsky, N.J., He, T., Zhang, F., Stockey, R.G., Cole, D.B., Lin, Y.B., Ling, H. F., 2021. Global marine redox evolution from the late Neoproterozoic to the early Paleozoic constrained by the integration of Mo and U isotope records. Earth-Science Rev. 214, 103506.
Wood, R.A., Poulton, S.W., Prave, A.R., Hoffmann, K.H., Clarkson, M.O., Guilbaud, R., Lyne, J.W., Tostevin, R., Bowyer, F., Penny, A.M., Curtis, A., Kasemann, S.A., 2015. Dynamic redox conditions control late Ediacaran metazoan ecosystems in the Nama Group, Namibia. *Precambrian Res.* 261, 252–271.
Xiao, S., Laflamme, M., 2009. On the eve of animal radiation: phylogeny, ecology and evolution of the Ediacara biota. Trends Ecol. Evol. 24, 31–40.
Yang, C., Rooney, A.D., Condon, D.J., Li, X.H., Grazhdankin, D.V., Bowyer, F.T., Hu, C., Macdonald, F.A., Zhu, M., 2021. The tempo of Ediacaran evolution. Sci. Adv. 7, 1–11.
Yang, B., Steiner, M., Zhu, M., Li, G., Liu, J., Liu, P., 2016. Transitional Ediacaran-Cambrian small skeletal fossil assemblages from South China and Kazakhstan: Implications for chronostratigraphy and metazoan evolution. Precambrian Res. 285, 202–215.
Zerkle, A.L., Junium, C.K., Canfield, D.E., House, C.H., 2008. Production of ^{15}N-depleted biomass during cyanobacterial N_2-fixation at high Fe concentrations. J. Geophys. Res. Biogeosciences 113, 1–9.
Zhang, K., Shields, G.A., 2023. Early diagenetic mobilization of rare earth elements and implications for the Ce anomaly as a redox proxy. Chem. Geol. 635, 121619.
Zhang, X., Sigman, D.M., Morel, F.M.M., Kraepiel, A.M.L., 2014. Nitrogen isotope fractionation by alternative nitrogenases and past ocean anoxia. Proc. Natl. Acad. Sci. U. S. A. 111, 4782–4787.
Zhang, F., Xiao, S., Kendall, B., Romaniello, S.J., Cui, H., Meyer, M., Gilleaudeau, G.J., Kaufman, A.J., Anbar, A.D., 2018. Extensive marine anoxia during the terminal Ediacaran Period. Sci. Adv. 4, 1–12.
Zhou, Y., Pogge von Strandmann, P.A.E., Zhu, M., Ling, H., Manning, C., Li, D., He, T., Shields, G.A., 2020. Reconstructing Tonian seawater $^{87}Sr/^{86}Sr$ using calcite microspar. Geology 48, 462–467.
Zhu, M.Y., Babcock, L.E., Peng, S.C., 2006. Advances in Cambrian stratigraphy and paleontology: Integrating correlation techniques, paleobiology, taphonomy and paleoenvironmental reconstruction. Palaeoworld 15, 217–222.
Zhu, M., Zhang, J., Steiner, M., Yang, A., Li, G., Erdtmann, B., 2003. Sinian-Cambrian stratigraphic framework for shallow- to deep-water environments of the Yangtze Platform: an integrated approach. Prog. Nat. Sci. 13, 951–960.
Zhu, M., Zhuravlev, A.Y., Wood, R.A., Zhao, F., Sukhov, S.S., 2017. A deep root for the Cambrian explosion: Implications of new bioand chemostratigraphy from the Siberian Platform. Geology 45, 459–462.
Zhu, M., Yang, A., Yuan, J., Li, G., Zhang, J., Zhao, F., Ahn, S.Y., Miao, L., 2019. Cambrian integrative stratigraphy and timescale of China. Sci. China Earth Sci. 62, 25–60.
Zhuravlev, A.Y., Liñán, E., Vintaned, J.A.G., Debrenne, F., Fedorov, A.B., 2012. New finds of skeletal fossils in the terminal Neoproterozoic of the Siberian Platform and Spain. Acta Palaeontol. Pol. 57, 205–224.